

DOI: 10.1002/ ((please add manuscript number))

Article type: Full Paper

Urea-modified Carbon Nitrides: Enhancing Photocatalytic Hydrogen Evolution by Rational Defect Engineering

*Vincent Wing-hei Lau, Victor Wen-zhe Yu, Florian Ehrat, Tiago Botari, Igor Moudrakovski, Thomas Simon, Viola Duppel, Elise Medina, Jacek Stolarczyk, Jochen Feldmann, Volker Blum, and Bettina V. Lotsch**

Dr. V.W. Lau, Dr I. Moudrakovski, V. Duppel, E. Medina, Prof. B.V. Lotsch Address line 1, Max Planck Institute for Solid State Research, Heisenbergstraße 1, 70569 Stuttgart, Germany
E-mail: b.lotsch@fkf.mpg.de

V.W. Yu, Dr. T. Botari, Prof. V. Blum
Department of Mechanical Engineering and Materials Science, Duke University, Durham, North Carolina 27708, USA

F. Ehrat, T. Simon, Dr. J. Stolarczyk, Prof. J. Feldmann
Photonics and Optoelectronics Group, Department of Physics and Center for Nanoscience (CeNS), Ludwig-Maximilians-Universität (LMU), Amalienstraße 54, 80799 Munich, Germany

F. Ehrat, T. Simon, Dr. J. Stolarczyk, Prof. J. Feldmann, Prof. B.V. Lotsch
Nanosystems Initiative Munich (NIM), Schellingstr. 4, 80799 Munich, Germany

Prof. B.V. Lotsch
Department of Chemistry, University of Munich, Butenandtstraße 5-13, 81377 Munich, Germany

Keywords: Graphitic Carbon Nitride, Photocatalysis, Solar Hydrogen, Rational Catalyst Design, Metal-Support Interaction

Abstract: The primary amine groups on the heptazine-based polymer melon, also known as graphitic carbon nitride (g-C₃N₄), can be replaced by urea groups using a two-step post-synthetic functionalization. Under simulated sunlight and optimum Pt loading, this urea-functionalized carbon nitride has one of the highest activities among organic and polymeric photocatalysts for hydrogen evolution with methanol as sacrificial donor, reaching an apparent quantum efficiency of 18% and nearly 30 times the hydrogen evolution rate compared to the non-functionalized counterpart. In the absence of Pt, the urea-derivatized material evolved hydrogen at a rate over four times that of the non-functionalized one. Since “defects” are conventionally accepted to be the active sites in graphitic carbon nitride for

1 photocatalysis, the work here is a demonstrated example of “defect engineering”, where the
2 catalytically relevant defect is inserted rationally for improving the intrinsic, rather than
3
4 extrinsic, photocatalytic performance. Furthermore, our work provides a retrodictive
5
6 explanation for the general observation that g-C₃N₄ prepared from urea performed better than
7
8 those prepared from dicyandiamide and melamine. In-depth analyses of the spent
9
10 photocatalysts and computational modelling suggest that inserting the urea group causes a
11
12 metal-support interaction (MSI) with the Pt co-catalyst, thus facilitating interfacial charge
13
14 transfer to the hydrogen evolving centers.
15
16
17
18
19
20
21

22 **1. Introduction**

23 Photocatalytic hydrogen evolution from water provides a direct method to capture and store
24
25 sunlight as chemical energy, which can then be released in an environmentally friendly
26
27 energy cycle. While a large library of photocatalytic materials has been catalogued^[1] in the
28
29 four decades since Honda’s and Fujishima’s report on photocatalytic water-splitting by
30
31 TiO₂,^[2] one of the most promising photocatalysts is the heptazine-based graphitic carbon
32
33 nitride (g-C₃N₄), historically known since Liebig’s era as melon.^[3] Melon is a 1-dimensional
34
35 polymer of heptazine, bridged by secondary amines, with neighbouring polymer strands
36
37 hydrogen-bonded together into quasi 2-dimensional arrays that form stacks through π - π
38
39 interaction (Scheme 1, left).^[4] Graphitic carbon nitride has also been depicted in the literature
40
41 as a fully condensed 2D layered structure with tertiary amines bridging every heptazine unit
42
43 (Scheme 1, middle),^[5] although this fully condensed material has not been unambiguously
44
45 shown to form experimentally to date. In 2009, the related yet fully 2-dimensionally linked
46
47 framework, poly(heptazine imide) or PHI, was reported (Scheme 1, right). PHI has a
48
49 hexagonal network where each heptazine forms three secondary amine bonds with
50
51 neighbouring heptazine units.^[6]
52
53
54
55
56
57
58
59
60
61
62
63
64
65

1 Graphitic carbon nitride as a photocatalyst has the advantages of being easily prepared from
2 inexpensive precursors (melamine, dicyandiamide or urea),^[7] having appropriate energy
3 levels straddling the redox potential required for water-splitting,^[8] functioning under visible
4 light irradiation, and being chemically stable. Overcoming one of its major disadvantages –
5 its still moderate activity – is the subject of research in the numerous reports on carbon nitride
6 photocatalysis. Most of the publications on graphitic carbon nitride thus far focus on three
7 main strategies for activity enhancement: 1) red-shifting the absorption onset through co-
8 polymerisation with dopant(s),^[9] 2) texturization for surface area increase,^[10] and 3)
9 composite formation with a (semi)conductor for improving photo-excited charge
10 separation.^[11] While useful, there is a striking lack of attempts to enhance the *intrinsic*
11 activity of carbon nitrides, which is aggravated by the limited molecular tunability of carbon
12 nitrides due to their insolubility and lack of reactivity. Here, the terms *intrinsic* and *extrinsic*
13 with respect to the catalytic properties are differentiated based on the definition proposed by
14 Vojvodic and Nørskov: intrinsic refers to the chemical composition and structure of the
15 catalyst material, whereas extrinsic refers to either geometrical structuring (strategy 2 above)
16 and/or its interface with another solid material, liquid or gas to influence the host catalyst
17 (strategy 3 above).^[12] At the same time, improving the interfacial transfer of photo-excited
18 charges to the reactants – via the co-catalyst – constitutes an important yet somewhat
19 overlooked strategy for improving photocatalytic activity.^[13] Even in the very efficient CdSe-
20 Pt system, it is estimated that only 40% of the photo-excited electrons are transferred to the
21 platinum from spherical CdSe particles,^[14] a prerequisite step for hydrogen evolution. We and
22 others have shown that the carbon nitride photocatalysts can function with a range of
23 hydrogen evolving electrocatalysts that are synthetic, biological or bio-inspired, with activity
24 rivalling that of platinum,^[15] even though the coupling between these catalysts and the
25 polymer is rather weak.^[15e] To address this, we have investigated the structural features that
26
27
28
29
30
31
32
33
34
35
36
37
38
39
40
41
42
43
44
45
46
47
48
49
50
51
52
53
54
55
56
57
58
59
60
61
62
63
64
65

1 lead to photocatalytic activity in amorphous melon as opposed to crystalline melon, which
2 exhibits negligible activity.^[16] Unlike crystalline melon, which is prepared in a sealed
3 ampoule under autogeneous ammonia pressure leading to reversible reaction conditions and
4 crystal defects healing, we have previously shown^[17] that amorphous melon contains crystal
5 imperfections in the form of dangling moieties resulting from incomplete cyclisation and
6 polymerisation, or impurities (e.g. oxygen) from the precursor. Using the methodology of
7 model photocatalysts, we identified the functional groups that may be considered as the
8 “defects” responsible for photocatalytic activity, namely the cyanamide moiety ($-\text{NCN}^-$) and
9 oxygen-bearing functional groups ($-\text{O}^-$, $-\text{COOH}$), which can be present due to incomplete
10 cyclization of the heptazine or incorporation of oxygen from the atmosphere or precursor.
11
12
13
14
15
16
17
18
19
20
21
22
23
24
25
26

27 Using this knowledge, we were furthermore able to demonstrate the concept of active site
28 engineering for activity improvement, that is, the rational insertion of the catalytically
29 relevant “defect” into the heptazine structure. This concept was illustrated by converting the
30 primary amines of melon into the anionic cyanamides, one of the “defects” identified,
31 through a post-synthetic treatment with KSCN to yield a material (henceforth notated as
32 NCN-CN_x ; see Scheme 2) outperforming melon by over 12 times at optimum Pt loading.^[17]
33
34 Note that, in Scheme 2, we have depicted only the site where the incorporated functional
35 group is present, which is either at every heptazine unit assuming a 1D polymeric heptazine
36 backbone, or at the periphery of the 2D network array of PHI (Scheme S1). The roles of such
37 “defects” may be to: 1) act as the reduction or oxidation reaction sites;^[18] 2) facilitate
38 intermolecular interactions to improve overall reaction kinetics through increased catalyst-
39 substrate affinity,^[15f] 3) modify energy levels or carrier dynamics,^[17] and/or 4) enable strong
40 photocatalyst/co-catalyst interactions to facilitate charge transfer.^[17]
41
42
43
44
45
46
47
48
49
50
51
52
53
54
55
56
57
58
59
60
61
62
63
64
65

1 As the cyanamide group can be hydrolyzed to urea,^[19] we here exploit this synthetic
2 procedure to introduce an oxygen-containing group into the heptazine polymer, since our
3 previous work identified oxy- or carboxylate as groups potentially relevant for
4 photocatalysis.^[17] The obvious advantage of this route is that, unlike heating the precursor in
5 oxygen or incorporating a dopant stochastically into the polymer, an oxygen-containing
6 moiety such as urea can be controllably inserted at the peripheral sites of the heptazine units,
7 thus facilitating characterization of the polymer for elucidating structure-activity relationship.
8 As will be shown here, this hydrolysis product – notated as urea-CN_x – exhibits
9 photocatalytic activity for hydrogen evolution outperforming even that of NCN-CN_x and
10 melon despite absorbing less in the visible region. The role of the urea moiety is rationalized
11 based on experimental and computational findings. Lastly, we provide a retrodictive
12 explanation of why melon has higher activity when synthesized from urea compared to
13 dicyandiamide or melamine^[20] based on the structural characterization of urea-CN_x. This
14 finding has particular importance given that a number of carbon nitride systems capable of
15 complete water splitting employed melon prepared from urea, while those prepared from
16 other precursors (e.g. dicyandiamide) exhibited low water-splitting activity.^[21] Hence, the
17 results herein highlight the implications of the approach of “defect engineering” for
18 systematically improving carbon nitride photocatalysts.

46 **2. Results & Discussions**

47 Since strong acids are known to catalyze the hydrolysis of cyanamides to form urea,^[19a] the
48 NCN-CN_x (experimental details in the supporting information) is assumed to undergo
49 hydrolysis at the cyanamide sites specifically when treated with HCl. This acid-treated
50 material, which we tentatively notate henceforth as urea-CN_x, was evaluated for
51 photocatalytic hydrogen evolution under simulated sunlight (AM1.5) under a range of
52 conditions, as shown in Figure 1. At the optimized Pt loading of 2 wt%, deposited in-situ by
53
54
55
56
57
58
59
60
61

1 the photo-reduction of H_2PtCl_6 , and using methanol (10 vol%) as the electron donor, the urea-
2 CN_x (20 mg) exhibited a stable hydrogen evolution rate of $56.2 \mu\text{mol h}^{-1}$ for over 100 h of
3 irradiation, more than doubled the stable rate of NCN-CN_x ($24.7 \mu\text{mol h}^{-1}$, optimized at
4 8 wt% Pt) and almost thirty times that of melon ($2.0 \mu\text{mol h}^{-1}$, optimized at 1 wt% Pt). In
5 terms of apparent quantum efficiency (AQE) at 400 nm, urea- CN_x has a value of 17.9%,
6 nearly double that of NCN-CN_x at 9.3% and nearly 36 times higher than that of melon at
7 0.5%. These performance metrics are summarized in Table S3; the action spectra of the three
8 catalysts are shown in Figure 2b. Though caution must be exercised when comparing
9 literature results,^[22] the urea- CN_x here exhibits one of the highest activities for the sacrificial
10 hydrogen evolution half reaction amongst organic and polymeric visible-light photocatalysts
11 (comparison with literature values given in Table S4) both in relative terms (i.e.
12 outperformance over a photocatalyst standard) as an IUPAC recommendation,^[23] or in
13 absolute terms using quantum efficiency as the performance metric as suggested by
14 researchers in the field.^[24] Note that higher quantum yields are generally obtained when
15 triethanolamine is used due to its more reductive potential, current doubling and other
16 effects;^[25] we nonetheless did not select this electron donor for activity benchmarking as it is
17 light sensitive, often contains optical impurities, and has a complex photo-oxidation
18 mechanism involving many intermediates,^[26] as compared to the well-studied, clean photo-
19 oxidation of methanol.^[27] Furthermore, we have also observed that a number of
20 photocatalysts exhibiting high activity with triethanolamine perform poorly with other
21 electron donors such as methanol (Table S4).

22
23
24
25
26
27
28
29
30
31
32
33
34
35
36
37
38
39
40
41
42
43
44
45
46
47
48
49
50
51
52
53 The urea- CN_x can evolve hydrogen photocatalytically using a range of different electron
54 donors (Figure 1c); in the absence of electron donor, trace amounts of hydrogen were
55 detected after over 12 h, albeit just over the detection limit of our GC. More significantly,
56
57
58
59
60
61
62
63
64
65

1 urea-CN_x evolved hydrogen photocatalytically even without the addition of Pt co-catalyst
2 (Figure 1d), with an average rate in the first 24 h of 17 nmol h⁻¹, over four times that of NCN-
3 CN_x (4.2 nmol h⁻¹) and melon (3.5 nmol h⁻¹). The apparent correlation between the BET
4 surface area and hydrogen evolution rate of urea-CN_x and melon suggests that surface area is
5 one key determinant for activity in the Pt-free case. Insertion of Pt co-catalyst, however,
6 changes the contribution of this factor substantially, as the surface area no longer sufficiently
7 accounts for the high activity of urea-CN_x. Based on the comparison of the hydrogen
8 evolution rate at optimized Pt loading normalized to the BET surface area, urea-CN_x evolves
9 hydrogen at a rate of 43.5 μmol h⁻¹ m⁻², far outperforming NCN-CN_x at 22.5 μmol h⁻¹ m⁻² and
10 melon at 6.1 μmol h⁻¹ m⁻², as summarized in Table S3. Notably, the superior photocatalytic
11 activity of urea-CN_x cannot be attributed to increased light collection since, from their action
12 spectra in Figure 2b, it has an absorption onset of around 435 nm, which is blue-shifted by
13 25 nm (0.15 eV) from that of melon and NCN-CN_x, both with onset at 460 nm. Rather, urea-
14 CN_x is utilizing the fewer absorbed photons far more efficiently for the desired redox reaction
15 than the other two samples, given that the solar irradiance peaks at around 500 nm.
16 Collectively, these observations point towards an intrinsic improvement in photocatalytic
17 performance which, as shown below, is attributable to the structural features of urea-CN_x and
18 their role in the photocatalytic reaction.

19 Urea-CN_x was characterized by spectroscopic methods and the results are shown in Figure 2.
20 All solid-state ¹³C and ¹⁵N NMR experiments (Figure 2c and d, respectively) were performed
21 using the sample prepared from isotope-enriched KS¹³C¹⁵N, with the enriched samples
22 showing identical FTIR spectra except for the isotope shifts (Figure S3), and compared
23 against ¹³C and ¹⁵N enriched urea. Urea-CN_x retained its heptazine character, as evidenced by
24 the ring-sextant out-of-plane bending vibration in the IR (809 cm⁻¹), the signals associated

1 with the central (-217.6 ppm) and outer heptazine nitrogen atoms (N1: -175.2 ppm) in the ¹⁵N
2 NMR spectra, as well as the inner (C2: 158.2 ppm) and outer (C1: 164.1 ppm) carbon atoms
3 in the ¹³C NMR spectra.^[28] The characteristic signals for the 2° amine bridging the heptazine
4 units are observable in the IR (1308 and 1212 cm⁻¹)^[29] and in the ¹⁵N spectra (N3: -240 ppm),
5 while the absence of a ¹⁵N signal at -265 ppm indicates the complete conversion of the melon
6 primary amine into cyanamide in the first step of Scheme 2.^[3a] The presence of the urea
7 group can be identified by its characteristic FTIR signals at 1653, 1579 and 1549 cm⁻¹, the
8 carbonyl signal (C3) at ≈166 ppm as a signal tail to signal C1, and the urea -NH₂ signal (N4)
9 at -290 ppm. Compared to urea, the ¹³C and ¹⁵N chemical shifts of urea-CN_x are slightly
10 shifted downfield, which we attribute to deshielding induced by the electron poor heptazine
11 ring. To confirm the NMR assignments, we performed cross polarization with polarization
12 inversion^[30] (CPPI, Figure 2e) and double correlation ¹H-¹⁵N-¹³C 2D NMR experiments
13 (Figure 2f). For the CPPI experiment, the lack of decay for N1 (outer heptazine nitrogen) and
14 N2 (central heptazine nitrogen) is consistent with the absence of directly bonded protons,
15 which identifies these nitrogens as the tertiary nitrogens of the heptazine ring. The decay of
16 N3 with a crossover point of ≈0 is consistent with the NH group, while the decay of N4 has a
17 crossover point of ≈-0.5 and is close to the theoretical value of -1/3 for NH₂. For the double
18 correlation experiment, long distance couplings are observed with the NMR parameters used.
19 Nonetheless, coupling of N4 to both C1 and C2 is consistent with a urea at a heptazine
20 terminal. From the elemental analysis (Table 1), the C:N atomic ratio of 0.70 for urea-CN_x is
21 consistent with both a 1D polymeric structure (Scheme S1 bottom left) and the idealized PHI
22 network structure (Scheme S1 bottom right) with a C:N ratio of <0.706. The near absence of
23 potassium signifies that the bulk of the compound is not ionic as in NCN-CN_x, although the
24 residual potassium can be associated with the presence of unreacted NCN-CN_x, which may
25 be buried within the polymer and inaccessible to the acid. This unreacted species is
26
27
28
29
30
31
32
33
34
35
36
37
38
39
40
41
42
43
44
45
46
47
48
49
50
51
52
53
54
55
56
57
58
59
60
61
62
63
64
65

discernible by the small FTIR signal at 2180 cm⁻¹ (see Figure S2 for enlarged spectra of this region), the broad signal between 125–102 ppm in the ¹³C spectrum (Figure 2c inset) and at ≈-280 ppm in the ¹⁵N spectrum, corresponding to the NCN moiety in NCN-CN_x.

Characterization of urea-CN_x by electron microscopy (TEM and SEM), XRD and sorption analyses (Figure 3) shows that this material consists of platelets with lateral dimensions of 40–80 nm. Its nanoscale morphology leads to a comparatively large BET surface area of nearly 65 m² g⁻¹ with mainly textural (inter-particle) porosity in the nanometer range, which was achieved without employing sacrificial hard templates. The short interlayer spacing of 3.2 Å and structural periodicity of 11 and 8.6 Å are observable in the TEM, XRD and electron diffraction patterns, and are identical to that of NCN-CN_x, indicating that the acid hydrolysis did not affect the general macroscopic structure. Additionally, like NCN-CN_x, urea-CN_x has around 20 wt% water based on its thermogravimetric analysis (Figure S3). Otherwise, one noticeable difference is the reduced *d*-spacing for urea-CN_x of 8.6 Å, compared to 9.0 Å for NCN-CN_x, a decrease which may be related to tighter packing as the urea group can form hydrogen bonds with neighboring heptazine units. As consistent with this explanation, we observe in the 2D ¹⁵N-¹³C spectrum that the urea NH₂ (N4) couples not only to the urea carbon C3 and the outer heptazine carbon C1, but also couples over longer distance to the inner heptazine carbon C2.

In order to analyze the charge transfer properties of urea-CN_x, the steady-state photoluminescence (PL) spectra were acquired for 1 mg mL⁻¹ aqueous suspensions of melon and urea-CN_x upon excitation at 375 nm (Figure 4a). The latter exhibited reduction of the PL signal by 83% compared to melon. Such inverse relationship between photocatalytic activity and PL intensity is commonly observed in many photocatalysts^[31] and is usually understood

1 in terms of a competition for photoexcited charges between the radiative and charge
2 separating channels. The charge transfer pathway leading to hydrogen generation can be
3 considered as an additional or more efficient non-radiative channel, leading to a decrease in
4 luminescence. The time-resolved PL measurements (Figure 4b) show a much faster PL decay
5 for urea-CN_x ($\tau_{1/e}$ lifetime of 0.77ns) than for melon ($\tau_{1/e}$ lifetime of 2.4ns). Taken together
6 with the reduced PL quantum yield of urea-CN_x, they indicate a 3-4 fold faster non-radiative
7 recombination rate in urea-CN_x than in melon, in agreement with the above interpretation.^[32]
8
9

10
11
12
13
14
15
16
17
18
19 Interestingly, as shown in Figure 4c (spectra shown in Figure S4), the addition of an electron
20 acceptor (decoration with Pt) or a hole acceptor (10 vol% methanol) to either of the two
21 materials results in only very moderate (10-15%) quenching of the PL; the apparent increases
22 in PL intensity upon addition of methanol to the platinized samples are within experimental
23 error. The corresponding PL decay traces (Figure 4d and e) show no change upon the
24 addition of Pt or methanol, even though the presence of a co-catalyst and a hole scavenger
25 strongly increases the photocatalytic efficiency. These results are unusual since in CdS-based
26 photocatalysts, for example, the decoration with co-catalyst strongly quenches PL and leads
27 to much faster signal decay.^[33] This suggests that in the first step the photoexcited charges
28 transfer to the internal site on the polymer, presumably the pendant primary amine and urea
29 moiety on melon and urea-CN_x, respectively. The lack of correlation between the PL decay
30 rate and the presence of Pt means that this initial step is independent (i.e. proceeds on a
31 different time scale) of the subsequent electron transfer to Pt and onwards to a proton, and
32 does not constitute the limiting step of the hydrogen generation process. Consequently, the
33 difference in photocatalytic efficiency between melon and urea-CN_x possibly arises from
34 different transfer rates from the internal site to the Pt particle (or directly a proton in case of a
35 non-platinized system), depending on the coupling between this site and the Pt particle.
36
37
38
39
40
41
42
43
44
45
46
47
48
49
50
51
52
53
54
55
56
57
58
59
60
61
62
63
64
65

1
2 To further explore the rationale for the high performance of urea-CN_x, namely the role of the
3
4 urea moiety and its interaction with the Pt co-catalyst, the spent catalyst with the Pt photo-
5
6 deposited in-situ after the 100+ hour photocatalytic experiment was fully characterized
7
8 (Figure 5). The FTIR and ¹³C NMR spectra and the XRD patterns are essentially identical
9
10 between the pristine and the spent catalyst, demonstrating chemical and morphological
11
12 stability of urea-CN_x after the photocatalytic reaction. In the ¹⁵N CP ssNMR spectrum,
13
14 appearance of peak shoulders for N1, N3 and possibly at N4 can be attributed to the presence
15
16 of the Pt co-catalyst and will be elaborated below. Similarly for the XPS, the general peak
17
18 shapes are largely unchanged after the photocatalytic reaction, although small shifts in the
19
20 binding energies are observed. Briefly, assignment of the deconvoluted XPS signals, based
21
22 on previous publications, is as follows. The signals for the heptazine sp² carbons and
23
24 nitrogens occur at 288.6 and 399.1 eV, while the sp³ nitrogen of the bridging 2° amine occurs
25
26 at 400.8 eV.^[34] The C1s signal at 286.5 eV may be assigned to the sp² carbon of urea, while
27
28 the broad signal at 293.6 eV is attributed to potassium associated with unreacted cyanamide
29
30 anion from NCN-CN_x. As illustrated in Figure 5, some C and N signals as well as the oxygen
31
32 signal from urea are shifted to higher binding energy (B.E.), with the oxygen shifting by
33
34 0.3 eV, well above the resolution of the XPS. For the in-situ deposited Pt, the Pt XPS 4f_{7/2}
35
36 signal can be deconvoluted into Pt²⁺ and Pt⁰ species as consistent with observation from
37
38 others^[35] and our previous research.^[17] While the B.E. of the Pt⁰ species (70.9 eV) is slightly
39
40 shifted compared to NCN-CN_x (71.1 eV) and melon (71.2 eV), the Pt²⁺ species at 71.9 eV,
41
42 which has been assigned in the literature to a PtO shell around the metallic Pt,^[35] is over
43
44 0.4 eV shifted to lower B.E. compared to NCN-CN_x (72.3 eV) and melon (72.4 eV).
45
46
47
48
49
50
51
52
53
54
55
56
57
58
59
60
61
62
63
64
65

1 shifts – towards higher B.E. for the carbon nitride and lower B.E. for the Pt – are in accord
2 with a metal-support interaction (MSI), specifically the donation of electron density from the
3 carbon nitride to the Pt.^[36] Given that both the oxygen and the Pt²⁺ XPS signals are shifted by
4 around the same magnitude but opposite direction, this would suggest that the urea moiety is
5 involved in connecting with the co-catalyst, facilitating charge transfer and thus leading to the
6 significant increase in photocatalytic hydrogen evolution. These XPS results are in fact
7 consistent with previous adsorption studies, which have found that the adsorption of urea
8 onto a Pt surface is accompanied by charge transfer from the adsorbate to the metal
9 surface.^[37]

10
11
12
13
14
15
16
17
18
19
20
21
22
23
24 Characterization by electron microscopy and diffraction (Figure 6 and Figure S5) showed not
25 only formation of Pt particles with diameter of 2–4 nm, but also that these particles seemingly
26 trace the edge of the platelets. This suggests that the urea-CN_x contained preferential sites for
27 Pt to coordinate to and to subsequently be reductively photo-deposited from H₂PtCl₆. In the
28 absence of more element specific techniques (XAS and electron tomography), our inference
29 consistent with our above ¹⁵N NMR and XPS findings as well as literature precedents is that
30 the urea moieties at the periphery are coordinating through the oxygen to the Pt cocatalyst.

31
32
33
34
35
36
37
38
39
40
41
42
43 As a final indicator, we use electronic structure theory to corroborate the implications derived
44 from the experimental observations above. We note that replicating the precise mechanistic
45 details of the photocatalyst and its operation by first-principles modelling would significantly
46 exceed the capabilities of any first-principles approaches currently available. However,
47 several key open questions that can be addressed relate to how the interaction with the Pt co-
48 catalyst *differs* between differently functionalized substrates, particularly melon and urea-
49 CN_x. These questions include: 1) the extent of the support/co-catalyst interaction; 2) the

1 moieties involved in the coordination to the Pt cluster; and 3) the potential for electron versus
2 hole transfer to the Pt cluster. Below, we approach these questions using still demanding, yet
3 feasible, ground state density-functional theory (DFT) based simulations. The findings here
4 aim to elucidate the characteristics that improve the electron transfer to the platinum, which
5 based on the above discussions appears to be the rate limiting step. It does not, however,
6 model the inherent carrier dynamics of the carbon nitrides, such as the processes related to
7 charge carrier separation or the percolation of charges inside the carbon nitride as discussed
8 in the PL section.
9
10
11
12
13
14
15
16
17
18
19
20
21

22 Specifically, we address questions 1-3 by comparing the electronic structure of two different
23 computational models of the substrate-Pt interaction, shown in Figure 7: (i) a Pt₁₃ cluster
24 adsorbed on a bilayer of melon (Fig. 7 a and c), and (ii) a Pt₁₃ cluster adsorbed on a
25 conceptual structural model of a bilayer of urea-CN_x (Fig. 7 b and d). While the structure of
26 melon layers is reasonably well established from past theory and experiment, we do not, at
27 this point, know the precise atomic structure of urea-CN_x planes. In order to facilitate a
28 meaningful comparison between both substrates, we therefore choose a computational
29 structure model for the urea-CN_x structure that allows us to focus specifically on the
30 differences that arise from replacing the NH₂ side chains of melon with the NH-CO-NH₂ side
31 chains of urea-CN_x. The chosen model substrate geometry of urea-CN_x is thus as similar as
32 possible to melon, i.e., a hydrogen-bonded bilayer model of 1D heptazine polymer strands,
33 but with all NH₂ groups replaced by urea moieties (see Scheme S1, bottom left). Both
34 structure models are realized as periodically repeated supercells. The unit cell dimension
35 perpendicular to the bilayers (*z* direction) is 40 Å, ensuring a large vacuum region.
36
37
38
39
40
41
42
43
44
45
46
47
48
49
50
51
52
53
54

55 Additionally, we employ a dipole correction^[38] in the *z* direction to prevent interactions
56 between different periodic images. The periodic images of the adsorbed Pt₁₃ clusters are
57
58
59
60
61
62
63
64
65

1 separated by using lateral supercell dimensions of four parallel heptazine strands with six
2 heptazine units along each strand in each layer. For the initial geometry of Pt₁₃, we chose a
3 minimum-energy structure determined by Piotrowski *et al.*^[39] The full bilayer models
4 including the Pt₁₃ cluster comprise a total of 877 atoms for melon and 1,069 atoms for urea-
5 CN_x. All atomic positions and lateral unit cell parameters were fully relaxed to the nearest
6 local minima of the potential-energy surface. The urea-CN_x model analyzed in Figure 7 b and
7 d is the lowest-energy model out of three different cluster-bilayer models that we tested for
8 urea-CN_x, all of which included the attachment of Pt₁₃ to O as an important feature. All
9 calculations were performed using the FHI-aims all-electron electronic structure code^[40],
10 “light” settings and the Γ point for Brillouin zone integration, and the Perdew-Burke-
11 Ernzerhof (PBE)^[41] density functional together with the Tkatchenko-Scheffler pairwise van
12 der Waals dispersion correction^[42] (PBE+vdW).

13
14
15
16
17
18
19
20
21
22
23
24
25
26
27
28
29
30
31 In Figure 7a) and b), we show the element-resolved partial densities of states of Pt₁₃ adsorbed
32 at the melon bilayer vs. at the urea-CN_x bilayer, respectively. We note that, without adsorbed
33 Pt₁₃ and in DFT-PBE, the melon bilayer would have a HOMO-LUMO gap of 2.53 eV,
34 whereas the Pt-free urea-CN_x bilayer would have a smaller HOMO-LUMO gap of 2.25 eV;
35 these values are consistent with the C-N band edges inferred from Figs. 7a) and b) when Pt₁₃
36 is present. Insets in both figures show the fully relaxed local Pt₁₃ adsorption geometry at
37 either substrate. Furthermore, the complete model geometries used for melon and urea-CN_x
38 are also shown in Figure 7c) and 7d), respectively, together with the orbital densities of two
39 particular hybridized states close to (at or just below) the substrate LUMO levels (see below).
40
41
42
43
44
45
46
47
48
49
50
51
52
53
54
55
56
57
58
59
60
61
62
63
64
65
66
67
68
69
70
71
72
73
74
75
76
77
78
79
80
81
82
83
84
85
86
87
88
89
90
91
92
93
94
95
96
97
98
99
100
101
102
103
104
105
106
107
108
109
110
111
112
113
114
115
116
117
118
119
120
121
122
123
124
125
126
127
128
129
130
131
132
133
134
135
136
137
138
139
140
141
142
143
144
145
146
147
148
149
150
151
152
153
154
155
156
157
158
159
160
161
162
163
164
165
166
167
168
169
170
171
172
173
174
175
176
177
178
179
180
181
182
183
184
185
186
187
188
189
190
191
192
193
194
195
196
197
198
199
200
201
202
203
204
205
206
207
208
209
210
211
212
213
214
215
216
217
218
219
220
221
222
223
224
225
226
227
228
229
230
231
232
233
234
235
236
237
238
239
240
241
242
243
244
245
246
247
248
249
250
251
252
253
254
255
256
257
258
259
260
261
262
263
264
265
266
267
268
269
270
271
272
273
274
275
276
277
278
279
280
281
282
283
284
285
286
287
288
289
290
291
292
293
294
295
296
297
298
299
300
301
302
303
304
305
306
307
308
309
310
311
312
313
314
315
316
317
318
319
320
321
322
323
324
325
326
327
328
329
330
331
332
333
334
335
336
337
338
339
340
341
342
343
344
345
346
347
348
349
350
351
352
353
354
355
356
357
358
359
360
361
362
363
364
365
366
367
368
369
370
371
372
373
374
375
376
377
378
379
380
381
382
383
384
385
386
387
388
389
390
391
392
393
394
395
396
397
398
399
400
401
402
403
404
405
406
407
408
409
410
411
412
413
414
415
416
417
418
419
420
421
422
423
424
425
426
427
428
429
430
431
432
433
434
435
436
437
438
439
440
441
442
443
444
445
446
447
448
449
450
451
452
453
454
455
456
457
458
459
460
461
462
463
464
465
466
467
468
469
470
471
472
473
474
475
476
477
478
479
480
481
482
483
484
485
486
487
488
489
490
491
492
493
494
495
496
497
498
499
500
501
502
503
504
505
506
507
508
509
510
511
512
513
514
515
516
517
518
519
520
521
522
523
524
525
526
527
528
529
530
531
532
533
534
535
536
537
538
539
540
541
542
543
544
545
546
547
548
549
550
551
552
553
554
555
556
557
558
559
560
561
562
563
564
565
566
567
568
569
570
571
572
573
574
575
576
577
578
579
580
581
582
583
584
585
586
587
588
589
590
591
592
593
594
595
596
597
598
599
600
601
602
603
604
605
606
607
608
609
610
611
612
613
614
615
616
617
618
619
620
621
622
623
624
625
626
627
628
629
630
631
632
633
634
635
636
637
638
639
640
641
642
643
644
645
646
647
648
649
650
651
652
653
654
655
656
657
658
659
660
661
662
663
664
665
666
667
668
669
670
671
672
673
674
675
676
677
678
679
680
681
682
683
684
685
686
687
688
689
690
691
692
693
694
695
696
697
698
699
700
701
702
703
704
705
706
707
708
709
710
711
712
713
714
715
716
717
718
719
720
721
722
723
724
725
726
727
728
729
730
731
732
733
734
735
736
737
738
739
740
741
742
743
744
745
746
747
748
749
750
751
752
753
754
755
756
757
758
759
760
761
762
763
764
765
766
767
768
769
770
771
772
773
774
775
776
777
778
779
780
781
782
783
784
785
786
787
788
789
790
791
792
793
794
795
796
797
798
799
800
801
802
803
804
805
806
807
808
809
810
811
812
813
814
815
816
817
818
819
820
821
822
823
824
825
826
827
828
829
830
831
832
833
834
835
836
837
838
839
840
841
842
843
844
845
846
847
848
849
850
851
852
853
854
855
856
857
858
859
860
861
862
863
864
865
866
867
868
869
870
871
872
873
874
875
876
877
878
879
880
881
882
883
884
885
886
887
888
889
890
891
892
893
894
895
896
897
898
899
900
901
902
903
904
905
906
907
908
909
910
911
912
913
914
915
916
917
918
919
920
921
922
923
924
925
926
927
928
929
930
931
932
933
934
935
936
937
938
939
940
941
942
943
944
945
946
947
948
949
950
951
952
953
954
955
956
957
958
959
960
961
962
963
964
965
966
967
968
969
970
971
972
973
974
975
976
977
978
979
980
981
982
983
984
985
986
987
988
989
990
991
992
993
994
995
996
997
998
999
1000

1 the NH₂ functionalities, which is slightly pulled out of the plane. In contrast, the urea-CN_x
2 bilayer model displays a substantial rearrangement of its atomic positions. In line with the
3 experimental conclusions, there is a direct attachment of Pt₁₃ to the O functionality of urea, as
4 well as a connection to several of the N atoms of different adjacent heptazine rings. We also
5 estimated the overall charge transfer from the substrates to the neutral Pt₁₃ cluster by
6 Mulliken and Hirshfeld^[43] atoms-in-molecules partitioning schemes. Both schemes indicate
7 practically no charge transfer from melon to Pt₁₃ (Mulliken: -0.18e, Hirshfeld: 0.0e), and a
8 small transfer of electrons to Pt₁₃ (Mulliken: -0.571e, Hirshfeld: -0.15e) for our particular
9 urea-CN_x-Pt₁₃ model.
10
11
12
13
14
15
16
17
18
19
20
21
22
23

24 We next turn to a closer analysis of the hybridization of Pt₁₃ states with the near-edge carrier
25 states of the substrates. Since the Pt₁₃ cluster is finite, the energies of its states found in the
26 band gaps of melon and urea-CN_x are discrete. We can therefore analyze the character of
27 each state near and in-between the substrate band edges by performing a Mulliken
28 decomposition into contributions from the Pt₁₃ cluster and contributions from the substrates.
29 The result of the state-resolved Mulliken analysis is shown in the bottom panels of Figures 7a
30 and c. For comparison, we also visualize the orbitals associated with all states close to or in-
31 between the band edges of Pt₁₃-melon and of Pt₁₃-urea-CN_x in the SI (Figure S8–S13). The
32 individual states are labelled by consecutive integer numbers. The number zero indicates the
33 state closest to the Fermi level, here taken to be the highest-energy state with an electronic
34 occupation greater than 0.5. Negative labels indicate filled states and positive numbers
35 indicate empty states. Based on the Mulliken analyses, we assign the state labelled “-26” in
36 the lower panel of Figure 7a) to the valence band maximum (VBM/HOMO) of melon. The
37 state labelled “6” in Figure 7a) is assigned to the conduction band minimum (CBM/LUMO)
38 of melon. Similarly, the states labelled “-34” and “1” in Figure 7b) are assigned as the
39
40
41
42
43
44
45
46
47
48
49
50
51
52
53
54
55
56
57
58
59
60
61
62
63
64
65

1 VBM/HOMO and CBM/LUMO of the urea-CN_x bilayer, respectively. However, states 2-4
2 are very close to state 1 in energy and are predominantly CN_x derived as well. They are thus
3 likely to be closely associated with the CBM/LUMO as well.
4
5
6

7
8
9 The discrete states in the band gaps of melon and of urea-CN_x are almost purely Pt₁₃-derived.
10 However, a few states near the band edges show a greater degree of hybridization. Let us first
11 analyze the electron-like states near the CBMs/LUMOs. For melon-Pt₁₃, a particular state of
12 interest is the partially hybridized state 5, just 0.2 eV below the apparent LUMO of melon.
13
14
15

16 The orbital density of this state is shown in Figure 7c). State 5 is strongly localized near the
17 Pt₁₃ cluster, but extends to a few heptazine units of the substrate. This or similar hybridized
18 states associated with the NH₂ moieties of melon could well serve as the states that facilitate
19 electron transfer to the Pt co-catalyst in general. The case of urea-CN_x is strikingly different
20 in that the states derived from its LUMO (just above the highest occupied level of the Pt
21 cluster) appear to be significantly more hybridized with the Pt states. As an example, Figure
22 7d) shows the orbital density for state 1 in the lower panel of Figure 7b), which is much more
23 extended along the strands near the Pt cluster than is the case for state 5 of Fig. 7c) (melon).
24
25
26
27
28
29
30
31
32
33
34
35
36
37
38
39
40
41
42
43
44
45
46
47
48
49
50
51
52
53
54
55
56
57
58
59
60
61
62
63
64
65

66
67
68
69
70
71
72
73
74
75
76
77
78
79
80
81
82
83
84
85
86
87
88
89
90
91
92
93
94
95
96
97
98
99
100

1
2 In summary, the results from our DFT-PBE+vdW model calculations are supportive of key
3
4 observations relating to the Pt-substrate interaction, specifically of an overall stronger metal-
5
6 support interaction for urea-CN_x, facilitated via O moieties, and of a stronger hybridization of
7
8 the electron-like states of urea-CN_x with Pt-derived states. The latter could be indicative of
9
10 more facile electron transfer pathways available in urea-CN_x than in the archetype melon.
11
12
13
14
15

16
17 Collectively, our results above may provide a retrodictive explanation to the observation that
18
19 melon prepared from urea, rather than from dicyandiamide or melamine, performed better
20
21 photocatalytically.^[20] The literature rationales for this observation have been attributed to
22
23 increased surface area^[20a] or increased condensation in the carbon nitride.^[20b] While the
24
25 former certainly contributes to the increased activity, Martin et al. have argued it does not
26
27 sufficiently account for the vast improvement observed.^[20b] Indeed, our results infer that the
28
29 higher activity observed in melon prepared from urea (henceforth notated as melon (urea)) as
30
31 compared to that from melamine is attributable to residual functional groups, namely the urea
32
33 moiety, from the incomplete cyclization and condensation of urea to heptazine via
34
35 dicyandiamide and melamine. For example, oxygen can be incorporated from
36
37 ureidomelamine,^[44] an impurity in melamine, or from trace water and oxygen in the synthesis
38
39 atmosphere. To verify our retrodiction, we prepared a sample of melon from urea for
40
41 comparison of the characterization results (Figure 8). As predicted, a small but nonetheless
42
43 discernible urea signal is observed in the ¹H-¹⁵N CP NMR at around -290 ppm for melon
44
45 (urea), which is absent for melon, and coincides with the urea NH₂ signal (N4) for urea-CN_x.
46
47
48 Furthermore, the spectra for melon (urea) resemble urea-CN_x more than those for melon,
49
50 particularly the apparent downfield shifts for the NMR signals of the heptazine core (N1 and
51
52 C2; N3 to a lesser extent).
53
54
55
56
57
58
59
60
61
62
63
64
65

1
2 In agreement with previous literature, we found that melon (urea), despite absorbing less in
3
4 the visible region as evident in their UV-Vis spectra (Figure 8c), performs better for
5
6 photocatalytic hydrogen evolution than melon: 4.4 vs 1.8 $\mu\text{mol h}^{-1}$ averaged over the first 8 h
7
8 under AM1.5 irradiation and 4.7% vs 0.5% AQE at 400 nm. We emphasize that these values
9
10 are still much lower than that of urea-CN_x or NCN-CN_x (56.2 $\mu\text{mol h}^{-1}$ and 24.7 $\mu\text{mol h}^{-1}$,
11
12 respectively). Through additional characterizations, we rule out as the principal factors for the
13
14 outperformance of urea-CN_x the variations in 1) BET surface area, 2) dispersibility in water
15
16 as measured by zeta potential, 3) Pt loading, and 4) Pt size, morphology and distribution (see
17
18 supporting information for detailed discussions). From this, we deduce that efficient charge
19
20 transfer mediated by the platinum/urea-CN_x interaction seems to be a key determinant for its
21
22 high activity. This work thus highlights the success of our “defect engineering” strategy by
23
24 the rational insertion of the activity-promoting functional group into the carbon nitride
25
26 backbone.
27
28
29
30
31
32
33
34
35
36

37 **3. Conclusion**

38 Treating melon in a KSCN melt followed by acid hydrolysis yielded a carbon nitride polymer
39
40 decorated with the urea functional group. This urea-CN_x exhibited one of the highest
41
42 photocatalytic activities for hydrogen evolution reported for carbon nitrides thus far, with
43
44 rates over twice that of the NCN-CN_x and over 28 times that of melon under simulated
45
46 sunlight using methanol as the electron donor. Likewise, the apparent quantum efficiency at
47
48 400 nm of this urea-CN_x (17.9%) is nearly twice that of NCN-CN_x (9.3%) and nearly 36
49
50 times that of melon (0.5%). We attribute this large improvement in activity primarily to the
51
52 rational insertion of the urea moiety which appears to be the preferential docking site for the
53
54 platinum co-catalyst and facilitate transfer of photo-generated charges into the hydrogen
55
56 evolving centers, based on results from TEM, XPS and computational modelling. Following
57
58
59
60
61
62
63
64
65

1 these results, we suggest a retrodictive explanation to the better photocatalytic performance
2 of melon prepared from urea compared to those from melamine and dicyandiamide. This
3 rationale was subsequently supported by experimental evidences and for the first time sheds
4 light on the role and nature of oxygen-containing catalytically relevant sites in carbon nitride
5 photocatalysts. Specifically, residual urea groups from incomplete heptazine cyclization and
6 decomposition were found in melon prepared from urea, which are not in detectable
7 abundance in the melon samples from melamine. The strategy presented herein can be
8 considered as an example of “functional defect design” or engineering of catalytically
9 relevant sites, where we deliberately inserted the photocatalytically relevant defect. The vast
10 increase in activity of this engineered sample attests to the success of this strategy which,
11 based on extensive characterization of the urea-CN_x, appears to be an even more promising
12 research direction for improving photocatalytic activity than red-shifting the absorption onset
13 or increasing the surface area, as it can subsequently be combined with all of these latter
14 strategies. Further exploration of mechanistic aspects, as well as exploring other defects
15 native or non-native to melon, may thus provide the design criteria for highly efficient
16 heptazine-based photocatalysts not only for the hydrogen evolution reaction, but also other
17 photoreactions demonstrated to be feasible for this material such as water oxidation, CO₂
18 reduction, and organic transformations.
19
20
21
22
23
24
25
26
27
28
29
30
31
32
33
34
35
36
37
38
39
40
41
42
43
44
45
46

47 **4. Experimental Section**

48 Details of the syntheses and characterization techniques are provided in the supporting
49 information. Computational results are provided in the NoMaD repository under the link
50 <http://dx.doi.org/10.17172/NOMAD/2016.11.14-1>; computationally calculated structures are
51 also uploaded in the supporting information as cif.
52
53
54
55
56
57
58
59

60 **Supporting Information**

Supporting Information is available from the Wiley Online Library or from the author.

Acknowledgements

V.W.-h.L. gratefully acknowledges a postdoctoral scholarship from the Max Planck Society. This work was supported by the Deutsche Forschungsgemeinschaft (project LO1801/1-1), the Max Planck Society, the cluster of excellence Nanosystems Initiative Munich (NIM), and the Center for Nanoscience (CeNS). Support from a seed grant by the Duke University Energy Initiative is gratefully acknowledged. The authors would like to thank Ms. Marie-Luise Schreiber for the elemental analyses, Dr. Mitsuharu Konuma for the XPS analyses, and Mr. Olaf Alberto von Mankowski for the argon sorption measurements.

Received: ((will be filled in by the editorial staff))

Revised: ((will be filled in by the editorial staff))

Published online: ((will be filled in by the editorial staff))

References

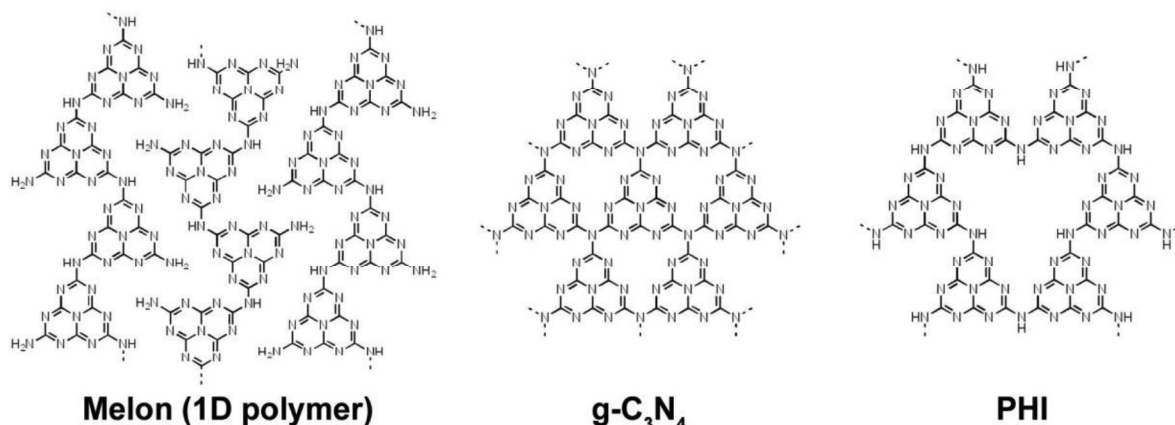
- [1] J. Xing, W. Q. Fang, H. J. Zhao, H. G. Yang, *Chem. Asian J.* **2012**, *7*, 642-657.
- [2] A. Fujishima, K. Honda, *Nature* **1972**, *238*, 37-38.
- [3] a) B. V. Lotsch, M. Döblinger, J. Sehnert, L. Seyfarth, J. Senker, O. Oeckler, W. Schnick, *Chem. Eur. J.* **2007**, *13*, 4969-4980; b) K. Maeda, X. Wang, Y. Nishihara, D. Lu, M. Antonietti, K. Domen, *J. Phys. Chem. C* **2009**, *113*, 4940-4947; c) X. Wang, K. Maeda, A. Thomas, K. Takanebe, G. Xin, J. M. Carlsson, K. Domen, M. Antonietti, *Nat. Mater.* **2009**, *8*, 76-80; d) S. Cao, J. Yu, *J. Phys. Chem. Lett.* **2014**, *5*, 2101-2107; e) J. Liu, H. Wang, M. Antonietti, *Chem. Soc. Rev.* **2016**, *45*, 2308-2326.
- [4] a) L. Seyfarth, J. Seyfarth, B. V. Lotsch, W. Schnick, J. Senker, *Phys. Chem. Chem. Phys.* **2010**, *12*, 2227-2237; b) T. Tyborski, C. Merschjann, S. Orthmann, F. Yang, M.-C. Lux-Steiner, T. Schedel-Niedrig, *J. Phys. Condens. Matter* **2013**, *25*, 395402; c) F. Fina, S. K. Callear, G. M. Carins, J. T. S. Irvine, *Chem. Mater.* **2015**, *27*, 2612-2618.
- [5] a) D. M. Teter, R. J. Hemley, *Science* **1996**, *271*, 53-55; b) E. Kroke, M. Schwarz, E. Horath-Bordon, P. Kroll, B. Noll, A. D. Norman, *New J. Chem.* **2002**, *26*, 508-512.
- [6] M. Döblinger, B. V. Lotsch, J. Wack, J. Thun, J. Senker, W. Schnick, *Chem. Commun.* **2009**, 1541-1543.

- 1
2
3
4
5
6
7
8
9
10
11
12
13
14
15
16
17
18
19
20
21
22
23
24
25
26
27
28
29
30
31
32
33
34
35
36
37
38
39
40
41
42
43
44
45
46
47
48
49
50
51
52
53
54
55
56
57
58
59
60
61
62
63
64
65
- [7] a) B. V. Lotsch, W. Schnick, *Chem. Mater.* **2006**, *18*, 1891-1900; b) A. Schwarzer, T. Saplinova, E. Kroke, *Coord. Chem. Rev.* **2013**, *257*, 2032-2062; c) B. V. Lotsch, W. Schnick, *New J. Chem.* **2004**, *28*, 1129-1136.
- [8] C. Butchosa, P. Guiglion, M. A. Zwijnenburg, *J. Phys. Chem. C* **2014**, *118*, 24833-24842.
- [9] a) G. Liu, P. Niu, C. Sun, S. C. Smith, Z. Chen, G. Q. M. Lu, H.-M. Cheng, *J. Am. Chem. Soc.* **2010**, *132*, 11642-11648; b) Y. Wang, Y. Di, M. Antonietti, H. Li, X. Chen, X. Wang, *Chem. Mater.* **2010**, *22*, 5119-5121; c) J. Zhang, X. Chen, K. Takanaabe, K. Maeda, K. Domen, J. D. Epping, X. Fu, M. Antonietti, X. Wang, *Angew. Chem. Int. Ed.* **2010**, *49*, 441-444; d) Y. Zhang, T. Mori, J. Ye, M. Antonietti, *J. Am. Chem. Soc.* **2010**, *132*, 6294-6295; e) J. Zhang, G. Zhang, X. Chen, S. Lin, L. Möhlmann, G. Dołęga, G. Lipner, M. Antonietti, S. Blechert, X. Wang, *Angew. Chem. Int. Ed.* **2012**, *51*, 3183-3187; f) Z. Lin, X. Wang, *Angew. Chem. Int. Ed.* **2013**, *52*, 1735-1738; g) K. Schwinghammer, B. Tuffy, M. B. Mesch, E. Wirnhier, C. Martineau, F. Taulelle, W. Schnick, J. Senker, B. V. Lotsch, *Angew. Chem. Int. Ed.* **2013**, *52*, 2435-2439.
- [10] a) X. Chen, Y.-S. Jun, K. Takanaabe, K. Maeda, K. Domen, X. Fu, M. Antonietti, X. Wang, *Chem. Mater.* **2009**, *21*, 4093-4095; b) P. Niu, L. Zhang, G. Liu, H.-M. Cheng, *Adv. Func. Mater.* **2012**, *22*, 2763-4770; c) J. Sun, J. Zhang, M. Zhang, M. Antonietti, X. Fu, X. Wang, *Nat. Commun.* **2012**, *3*, 1139; d) X. Wang, K. Maeda, X. Chen, K. Takanaabe, K. Domen, Y. Hou, X. Fu, M. Antonietti, *J. Am. Chem. Soc.* **2009**, *131*, 1680-1681.
- [11] Z. Zhao, Y. Sun, F. Dong, *Nanoscale* **2015**, *7*, 15-37.
- [12] A. Vojvodic, J. K. Nørskov, *Natl. Sci. Rev.* **2015**, *2*, 140-149.
- [13] P. V. Kamat, *J. Phys. Chem. Lett.* **2012**, *3*, 663-672.
- [14] C. Harris, P. V. Kamat, *ACS Nano* **2010**, *4*, 7321-7330.

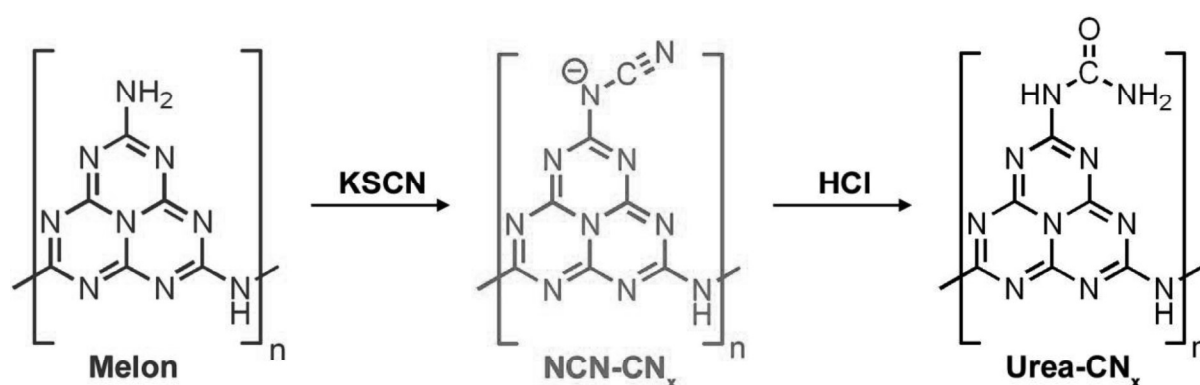
- 1
2
3
4
5
6
7
8
9
10
11
12
13
14
15
16
17
18
19
20
21
22
23
24
25
26
27
28
29
30
31
32
33
34
35
36
37
38
39
40
41
42
43
44
45
46
47
48
49
50
51
52
53
54
55
56
57
58
59
60
61
62
63
64
65
- [15] a) J. Dong, M. Wang, X. Li, L. Chen, Y. He, L. Sun, *ChemSusChem* **2012**, *5*, 2133-2138; b) S.-W. Cao, X.-F. Liu, Y.-P. Yuan, Z.-Y. Zhang, J. Fang, S. C. J. Loo, J. Barber, T. C. Sum, C. Xue, *Phys. Chem. Chem. Phys.* **2013**, *15*, 18363-18366; c) J. Hong, Y. Wang, Y. Wang, W. Zhang, R. Xu, *ChemSusChem* **2013**, *6*, 2263-2268; d) S.-W. Cao, Y.-P. Yuan, J. Barber, S. C. J. Loo, C. Xue, *Appl. Surf. Sci.* **2014**, *319*, 344-349; e) C. A. Caputo, M. A. Gross, V. W. Lau, C. Cavazza, B. V. Lotsch, E. Reisner, *Angew. Chem. Int. Ed.* **2014**, *53*, 11538-11542; f) H. Kasap, C. A. Caputo, B. C. M. Martindale, R. Godin, V. W.-H. Lau, B. V. Lotsch, J. R. Durrant, E. Reisner, *J. Am. Chem. Soc.* **2016**, *138*, 9183-9192.
- [16] V. W.-h. Lau, M. B. Mesch, V. Duppel, V. Blum, J. Senker, B. V. Lotsch, *J. Am. Chem. Soc.* **2015**, *137*, 1064-1072.
- [17] V. W.-h. Lau, I. Moudrakovski, T. Botari, S. Weinberger, M. B. Mesch, V. Duppel, J. Senker, V. Blum, B. V. Lotsch, *Nat. Commun.* **2016**, *7*, 12165.
- [18] Y. Wang, X. Wang, M. Antonietti, *Angew. Chem. Int. Ed.* **2012**, *51*, 68-89.
- [19] a) T. G uthner, B. Mertschenk, in *Ullmann's Encyclopedia of Industrial Chemistry*, **2006**; b) M. L. Kilpatrick, *J. Am. Chem. Soc.* **1947**, *69*, 40-46.
- [20] a) Y. Zhang, J. Liu, G. Wu, W. Chen, *Nanoscale* **2012**, *4*, 5300-5303; b) D. J. Martin, K. Qiu, S. A. Shevlin, A. D. Handoko, X. Chen, Z. Guo, J. Tang, *Angew. Chem.* **2014**, *53*, 9240-9245.
- [21] a) J. Liu, Y. Liu, N. Liu, Y. Han, X. Zhang, H. Huang, Y. Lifshitz, S.-T. Lee, J. Zhong, Z. Kang, *Science* **2015**, *347*, 970-974; b) G. Zhang, Z.-A. Lan, L. Lin, S. Lin, X. Wang, *Chem. Sci.* **2016**, *7*, 3062-3066.
- [22] T. Maschmeyer, M. Che, *Angew. Chem. Int. Ed.* **2010**, *49*, 1536-1539.
- [23] a) A. Salinaro, A. V. Emeline, J. Zhao, H. Hidaka, V. K. Ryabchuk, N. Serpone, *Pure Appl. Chem.* **1999**, *71*, 321-335; b) N. Serpone, A. Salinaro, *Pure Appl. Chem.* **1999**, *71*, 303-320.

- 1
2
3
4
5
6
7
8
9
10
11
12
13
14
15
16
17
18
19
20
21
22
23
24
25
26
27
28
29
30
31
32
33
34
35
36
37
38
39
40
41
42
43
44
45
46
47
48
49
50
51
52
53
54
55
56
57
58
59
60
61
62
63
64
65
- [24] H. Kisch, D. Bahnemann, *J. Phys. Chem. Lett.* **2015**, *6*, 1907-1910.
- [25] M. J. Berr, P. Wagner, S. Fischbach, A. Vaneski, J. Schneider, A. S. Susha, A. L. Rogach, F. Jäckel, J. Feldmann, *Appl. Phys. Lett.* **2012**, *100*, 223903.
- [26] S. Horikoshi, N. Watanabe, M. Mukae, H. Hidaka, N. Serpone, *New J. Chem.* **2001**, *25*, 999-1005.
- [27] F. Guzman, S. S. C. Chuang, C. Yang, *Ind. Eng. Chem. Res.* **2013**, *52*, 61-65.
- [28] B. Jürgens, E. Irran, J. Senker, P. Kroll, H. Müller, W. Schnick, *J. Am. Chem. Soc.* **2003**, *125*, 10288-10300.
- [29] T. Komatsu, *J. Mater. Chem.* **2001**, *11*, 799-801.
- [30] C. Gervais, F. Babonneau, J. Maquet, C. Bonhomme, D. Massiot, E. Framery, M. Vaultier, *Magn. Reson. Chem.* **1998**, *36*, 407-414.
- [31] M. Shalom, S. Inal, C. Fettkenhauer, D. Neher, M. Antonietti, *J. Am. Chem. Soc.* **2013**, *135*, 7118-7121.
- [32] a) D. Hollmann, M. Karnahl, S. Tschierlei, K. Kailasam, M. Schneider, J. r. Radnik, K. Grabow, U. Bentrup, H. Junge, M. Beller, S. Lochbrunner, A. Thomas, A. Brückner, *Chem. Mater.* **2014**, *26*, 1727-1733; b) H. Zhang, A. Yu, *J. Phys. Chem. C* **2014**, *118*, 11628-11635.
- [33] a) K. Wu, T. Lian, *Chem. Soc. Rev.* **2016**, *45*, 3781-3810; b) T. Simon, N. Bouchonville, M. J. Berr, A. Vaneski, A. Adrović, D. Volbers, R. Wyrwich, M. Döblinger, A. S. Susha, A. L. Rogach, F. Jäckel, J. K. Stolarczyk, J. Feldmann, *Nat. Mater.* **2014**, *13*, 1013-1018.
- [34] A. Thomas, A. Fischer, F. Goettmann, M. Antonietti, J.-O. Müller, R. Schlögl, J. M. Carlsson, *J. Mater. Chem.* **2008**, *18*, 4893-4908.
- [35] F. Fina, H. Ménard, J. T. S. Irvine, *Phys. Chem. Chem. Phys.* **2015**, *17*, 13929-13936.
- [36] a) P. Bera, K. R. Priolkar, A. Gayen, P. R. Sarode, M. S. Hegde, S. Emura, R. Kumashiro, V. Jayaram, G. N. Subbanna, *Chem. Mater.* **2003**, *15*, 2049-2060; b) F. Zhang, J.

- 1
2
3
4
5
6
7
8
9
10
11
12
13
14
15
16
17
18
19
20
21
22
23
24
25
26
27
28
29
30
31
32
33
34
35
36
37
38
39
40
41
42
43
44
45
46
47
48
49
50
51
52
53
54
55
56
57
58
59
60
61
62
63
64
65
- Chen, X. Zhang, W. Gao, R. Jin, N. Guan, Y. Li, *Langmuir* **2004**, *20*, 9329-9334; c) Y. Nagai, T. Hirabayashi, K. Dohmae, N. Takagi, T. Minami, H. Shinjoh, S. Matsumoto, *J. Catal.* **2006**, *242*, 103-109; d) A. Lewera, L. Timperman, A. Roguska, N. Alonso-Vante, *J. Phys. Chem. C* **2011**, *115*, 20153-20159; e) N. G. Akalework, C.-J. Pan, W.-N. Su, J. Rick, M.-C. Tsai, J.-F. Lee, J.-M. Lin, L.-D. Tsaic, B.-J. Hwang, *J. Mater. Chem.* **2012**, *22*, 20977-20985.
- [37] a) V. Climent, A. Rodes, R. Albalat, J. Claret, J. M. Feliu, A. Aldaz, *Langmuir* **2001**, *17*, 8260-8269; b) M. García-Hernández, U. Birkenheuer, A. Hu, F. Illas, N. Rösch, *Surf. Sci.* **2001**, *471*, 151-162.
- [38] J. Neugebauer, M. Scheffler, *Physical review. B, Condensed matter* **1992**, *46*, 16067-16080.
- [39] M. J. Piotrowski, P. Piquini, J. L. F. Da Silva, *Physical Review B* **2010**, *81*, 155446.
- [40] a) V. Blum, R. Gehrke, F. Hanke, P. Havu, V. Havu, X. Ren, K. Reuter, M. Scheffler, *Comput. Phys. Commun.* **2009**, *180*, 2175-2196; b) V. Havu, V. Blum, P. Havu, M. Scheffler, *J. Comput. Phys.* **2009**, *228*, 8367-8379; c) F. Knuth, C. Carbogno, V. Atalla, V. Blum, M. Scheffler, *Comput. Phys. Commun.* **2015**, *190*, 33-50; d) A. Marek, V. Blum, R. Johanni, V. Havu, B. Lang, T. Auckenthaler, A. Heinecke, H.-J. Bungartz, H. Lederer, *J. Phys. Condens. Matter* **2014**, *26*, 213201.
- [41] J. P. Perdew, K. Burke, M. Ernzerhof, *Phys. Rev. Lett.* **1996**, *77*, 3865-3868.
- [42] A. Tkatchenko, M. Scheffler, *Phys. Rev. Lett.* **2009**, *102*, 073005.
- [43] F. L. Hirshfeld, *Theoretica Chimica Acta* **1977**, *44*, 129-138.
- [44] M. Himmelsbach, T. D. T. Vo, *Electrophoresis* **2014**, *35*, 1362-1367.



14 **Scheme 1.** Structures of “graphitic carbon nitrides”. Shown are the 1D polymer melon (left),
15 the fully condensed 2D counterpart (middle), and the 2D network PHI.



31 **Scheme 2.** Simplified reaction scheme of the compound synthesized in this work, showing
32 melon and its conversion to NCN-CN_x by a post-synthetic reaction using KSCN melt, and its
33 acid-induced hydrolysis to urea-CN_x.

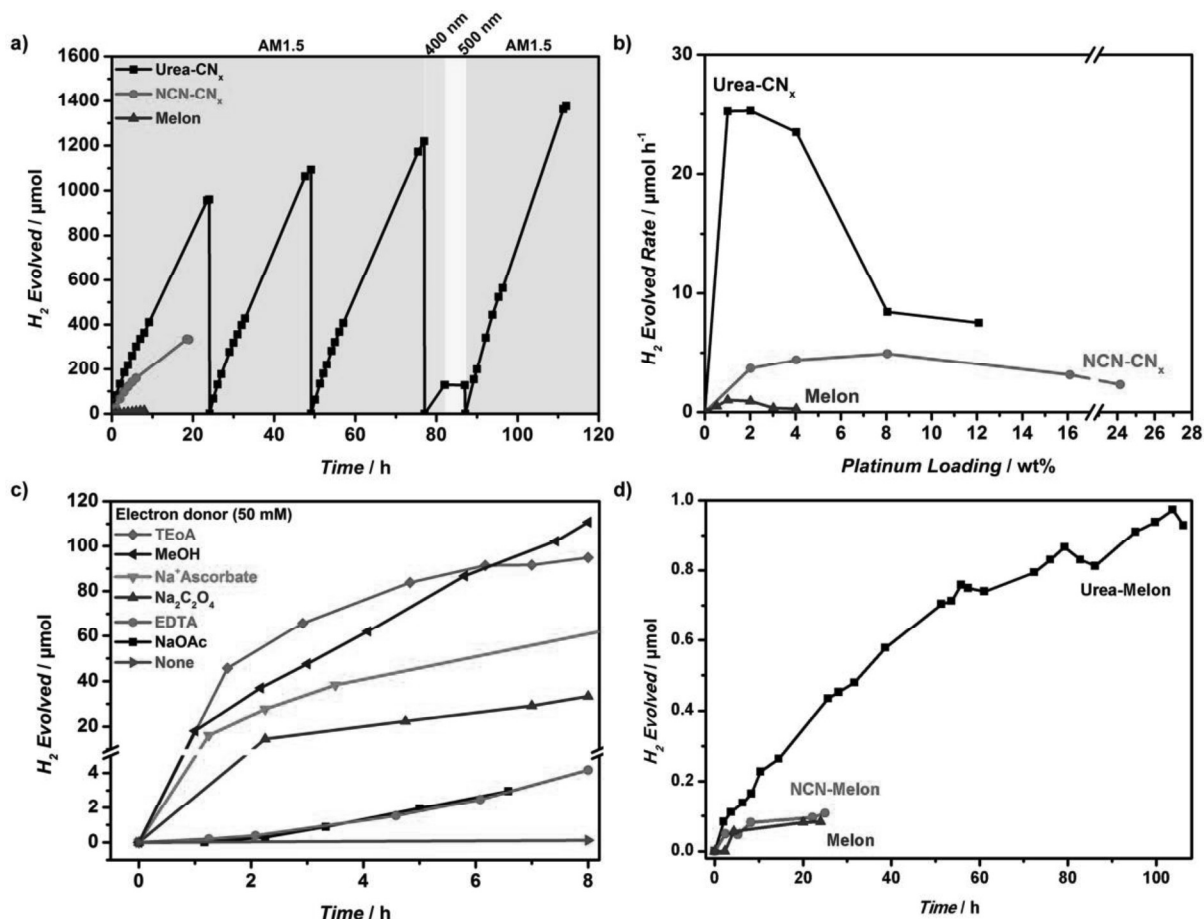


Figure 1. a) Photocatalytic hydrogen evolution under AM1.5, 400 nm or 500 nm band pass irradiation using methanol (10 vol%) as electron donor at the optimized Pt loading. Reactor headspace was purged after every overnight cycle, and methanol (200 μL) was added on the 24th and 87th hour. Since the gas chromatograph is operated manually, sampling is done at irregular intervals to give the illusion that the rate is increasing. b) Optimization of hydrogen evolution rate to Pt loading. c) Hydrogen evolution under AM1.5 irradiation and optimized Pt loading using different electron donors (50 mM); note that the non-linearity of some plots are due to the break in the y-axis. d) Photocatalytic hydrogen evolution without Pt co-catalyst under AM1.5 irradiation, using aqueous methanol as electron donor (10 vol%); note that some plots appear erratic as the amounts of hydrogen evolved were small and may be affected by frequent sampling.

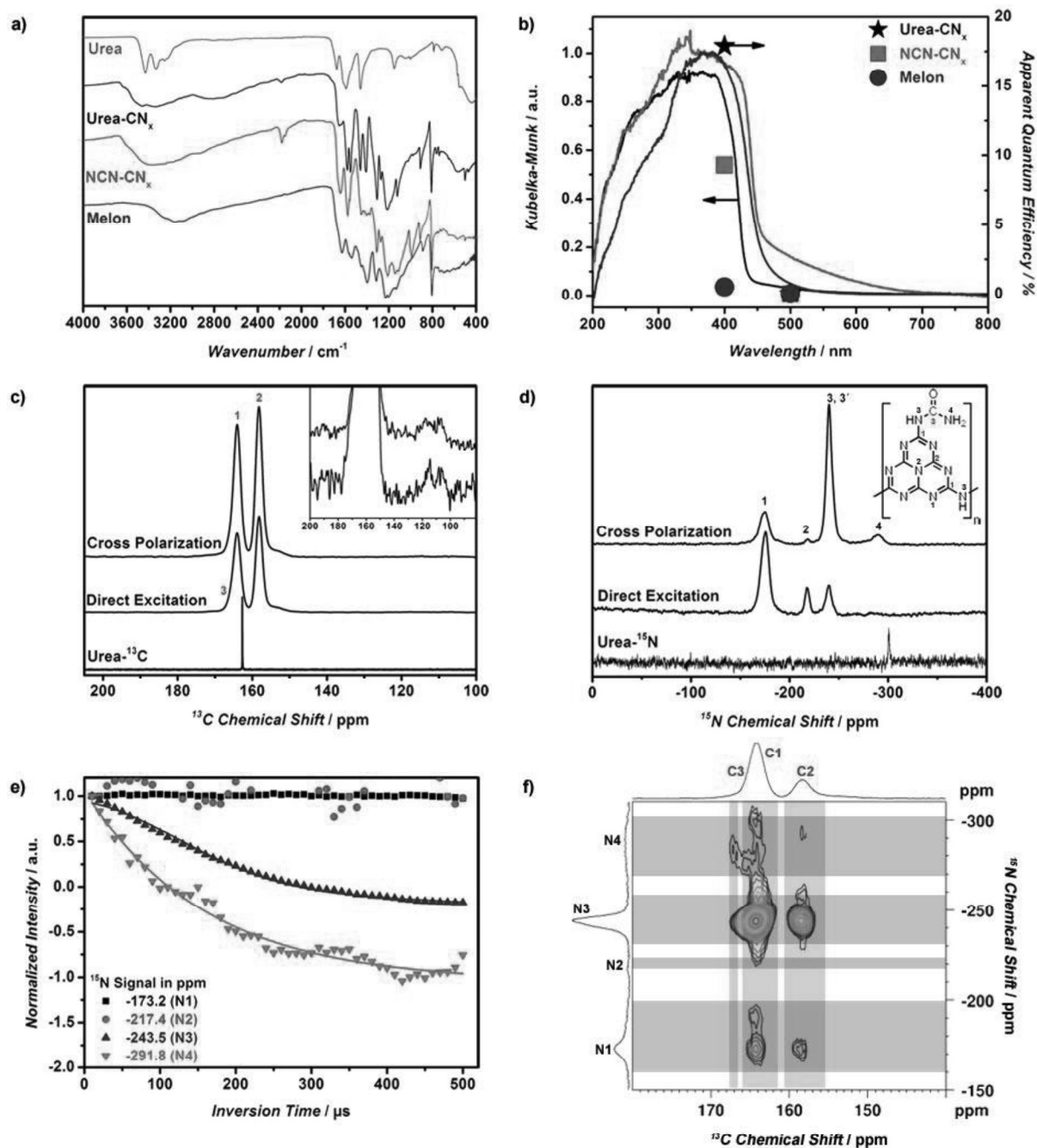


Figure 2. Spectroscopic characterization of urea-CN_x: a) FTIR (enlarged spectra in the 2400–1400 cm⁻¹ range shown in Figure S2); b) action spectrum compared to those of NCN-CN_x and melon; c) ¹³C and d) ¹⁵N magic angle spinning solid state NMR with either ¹H cross polarization or direct excitation; inset of c is an enlarged version showing the minute ¹³C cyanamide signal, while the inset of d shows the proposed structure of urea-CN_x and the NMR assignment; e) evolution of signal integrals vs inversion time in the ¹⁵N CPPI experiment and estimation of the turning points, f) ¹⁵N-¹³C 2D spectrum of the ¹H→¹⁵N, ¹⁵N→¹³C double cross polarization experiment. Comparisons of the ¹³C and ¹⁵N NMR spectra were made with ¹⁵N-enriched urea in D₂O. Deconvolution of the N3 signal in the ¹⁵N CP NMR is shown in Figure S2.

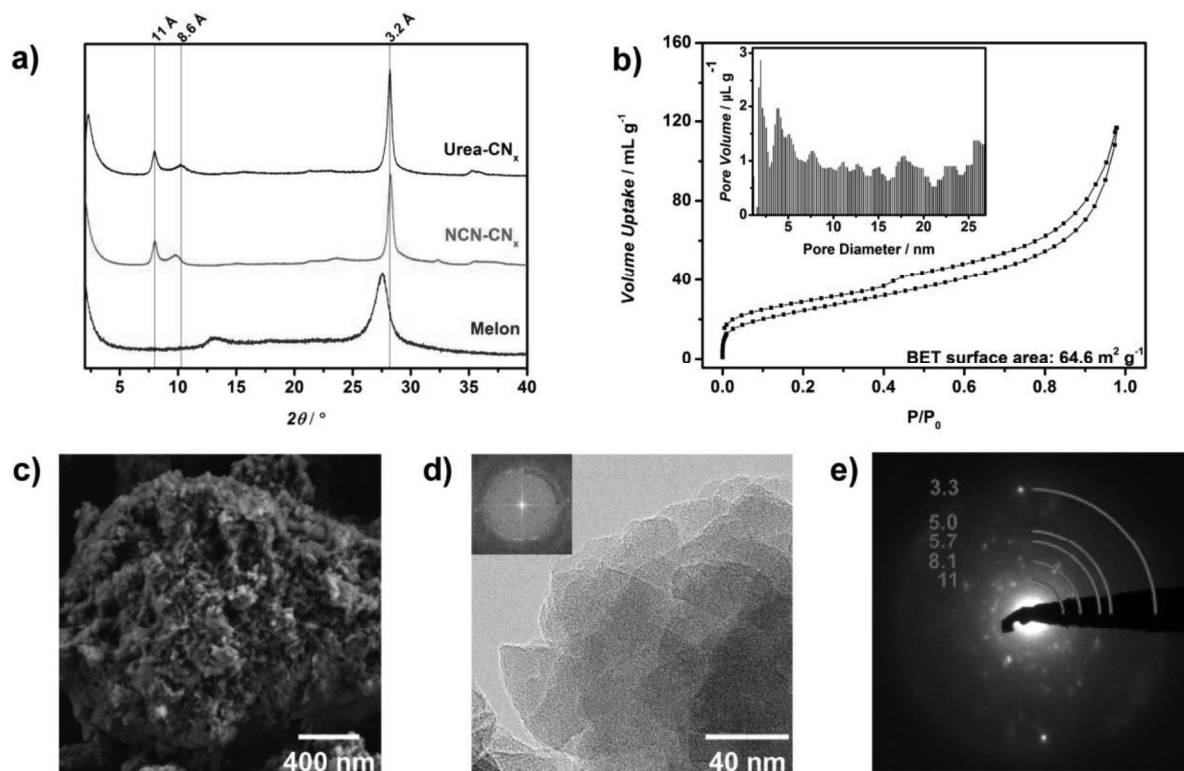


Figure 3. Characterization of urea-CN_x: a) XRD pattern of urea-CN_x compared with those of NCN-CN_x and melon; b) argon sorption isotherm and pore size distribution (inset); c) SEM; d) TEM and its fast Fourier transform (inset), where the red quarter circle shows a *d*-spacing of 10.4 Å, and e) electron diffraction pattern, where the quarter circles show *d*-spacings in Å.

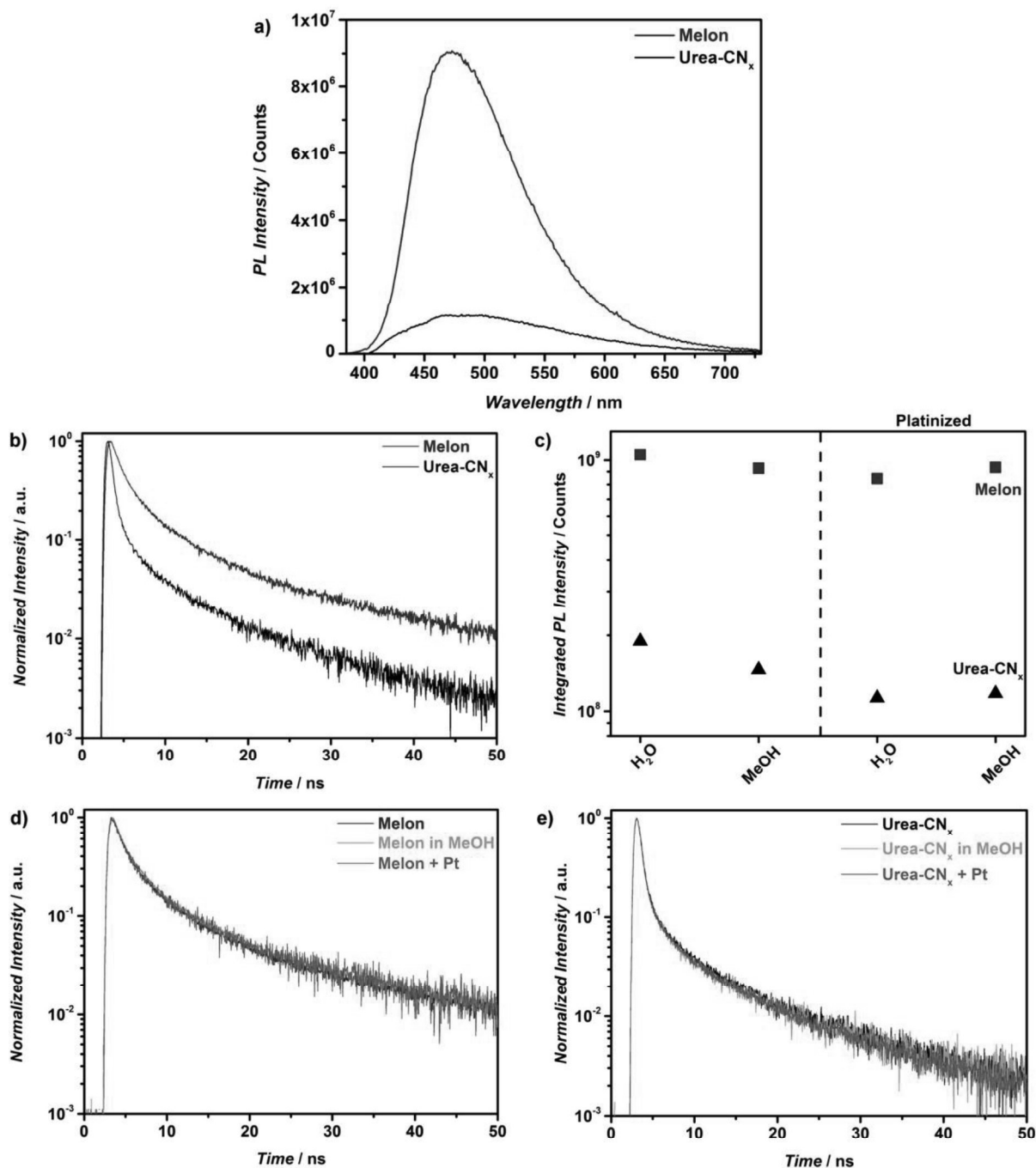
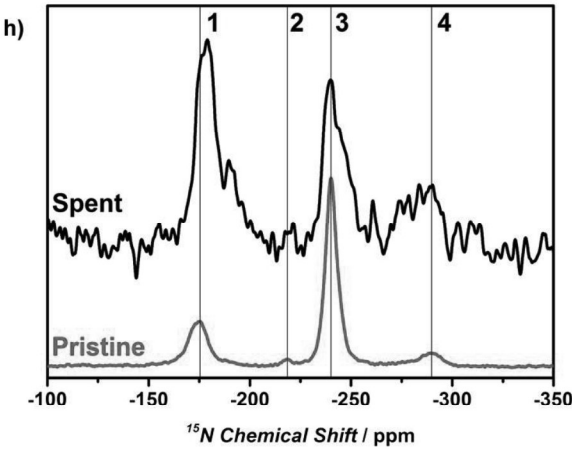
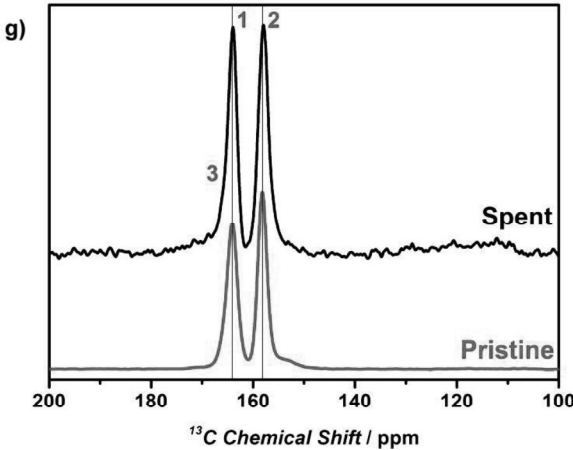
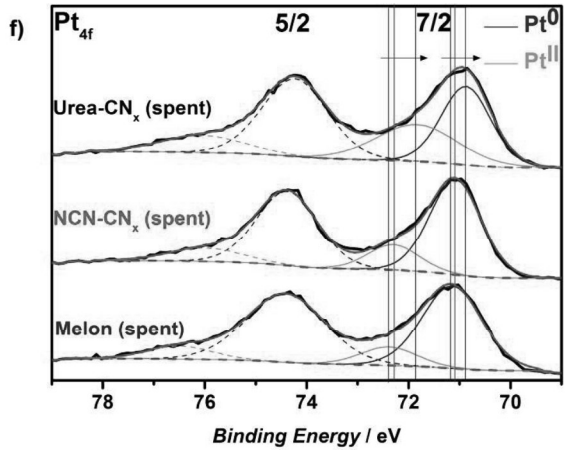
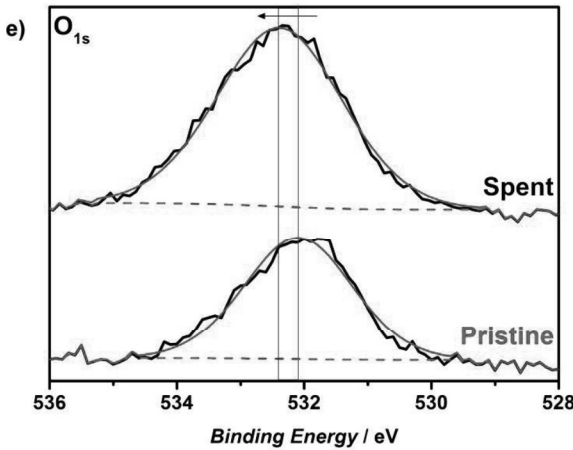
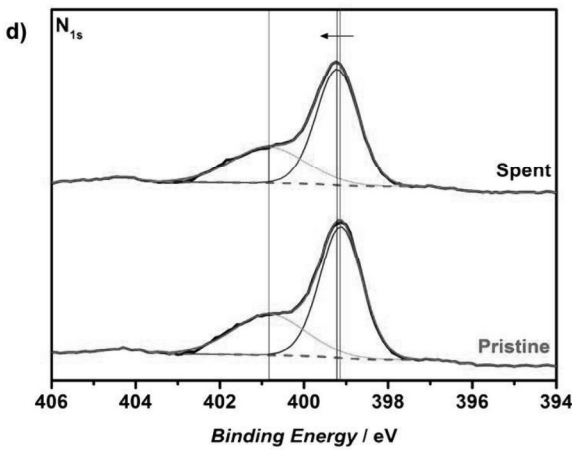
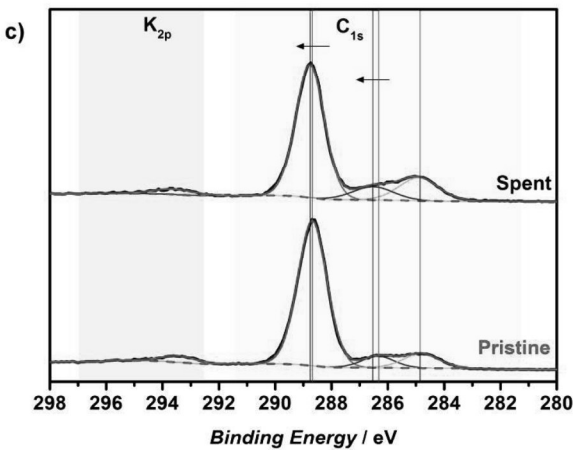
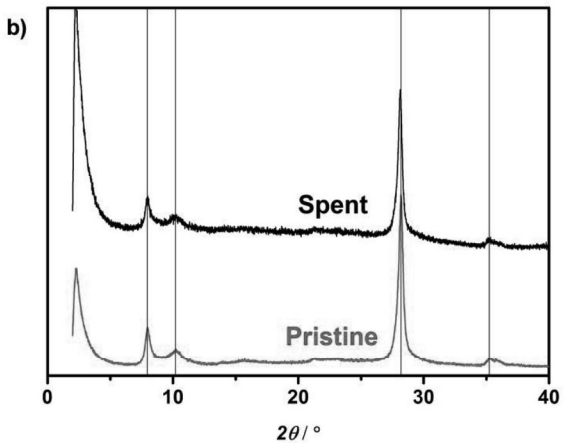
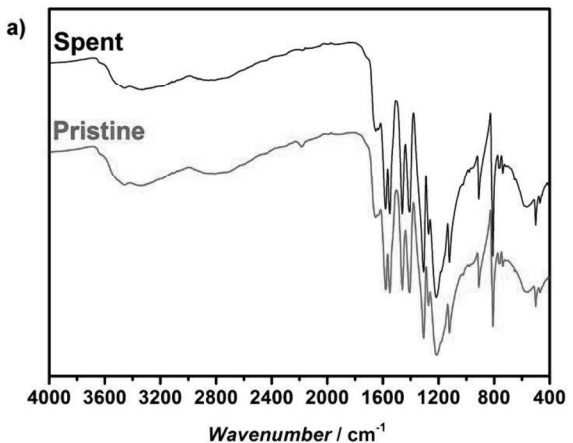
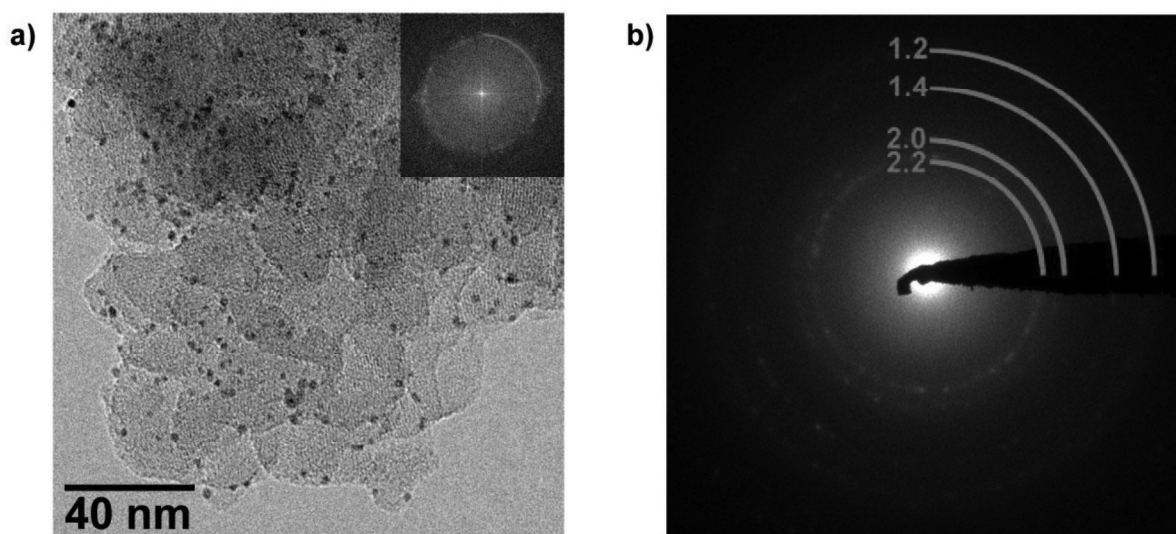


Figure 4. a) PL spectra with excitation at 375 nm of aqueous suspensions of melon and urea-CN_x; b) PL decay curves of melon and urea-CN_x; c) comparison of the PL intensity for melon and urea-CN_x under different environments based on the integral of the PL signal; comparison of PL decay curves of melon (d) and urea-CN_x (e) in the presence of the electron (Pt) or hole acceptor (MeOH).

1
2
3
4
5
6
7
8
9
10
11
12
13
14
15
16
17
18
19
20
21
22
23
24
25
26
27
28
29
30
31
32
33
34
35
36
37
38
39
40
41
42
43
44
45
46
47
48
49
50
51
52
53
54
55
56
57
58
59
60
61
62
63
64
65



1 **Figure 5.** Characterization of the spent photocatalyst compared to the pristine material by: a)
2 FTIR; b) XRD; XPS spectrum referenced to adventitious carbon at 284.8 eV in the K_{2p} and
3 C_{1s} (c), N_{1s} (d), O_{1s} (e) and Pt_{4f} (f) regions. For (c) to (e), the black and red hairlines
4 correspond respectively to the spent and pristine urea-CN_x, while for (f) the black, red and
5 black hairlines correspond to urea-CN_x, NCN-CN_x and melon, respectively. For (c) to (e), the
6 direction of the peak(s) shift of the spent compared to the pristine catalyst is indicated by the
7 arrow. For (f), the arrows show the direction of the peak shift going from melon to NCN-CN_x
8 to urea-CN_x. ¹³C direct excitation (g), and ¹⁵N CP (h) MAS ssNMR. Since only changes in
9 the chemical environments, rather than their quantification, are of interest in the NMR spectra,
10 the spent catalyst with natural isotopic abundance is compared with the pristine one from
11 Figure 2, which has 99% ¹³C and ¹⁵N isotope enrichment.
12
13



33 **Figure 6.** Electron microscopy analyses of the urea-CN_x after 100+ h photocatalysis: a) TEM
34 and the FFT with the quarter circle indicating a *d*-spacing of 11 Å (inset); b) electron
35 diffraction pattern showing the *d*-spacings in Å of Pt.
36
37
38
39
40
41
42
43
44
45
46
47
48
49
50
51
52
53
54
55
56
57
58
59
60
61
62
63
64
65

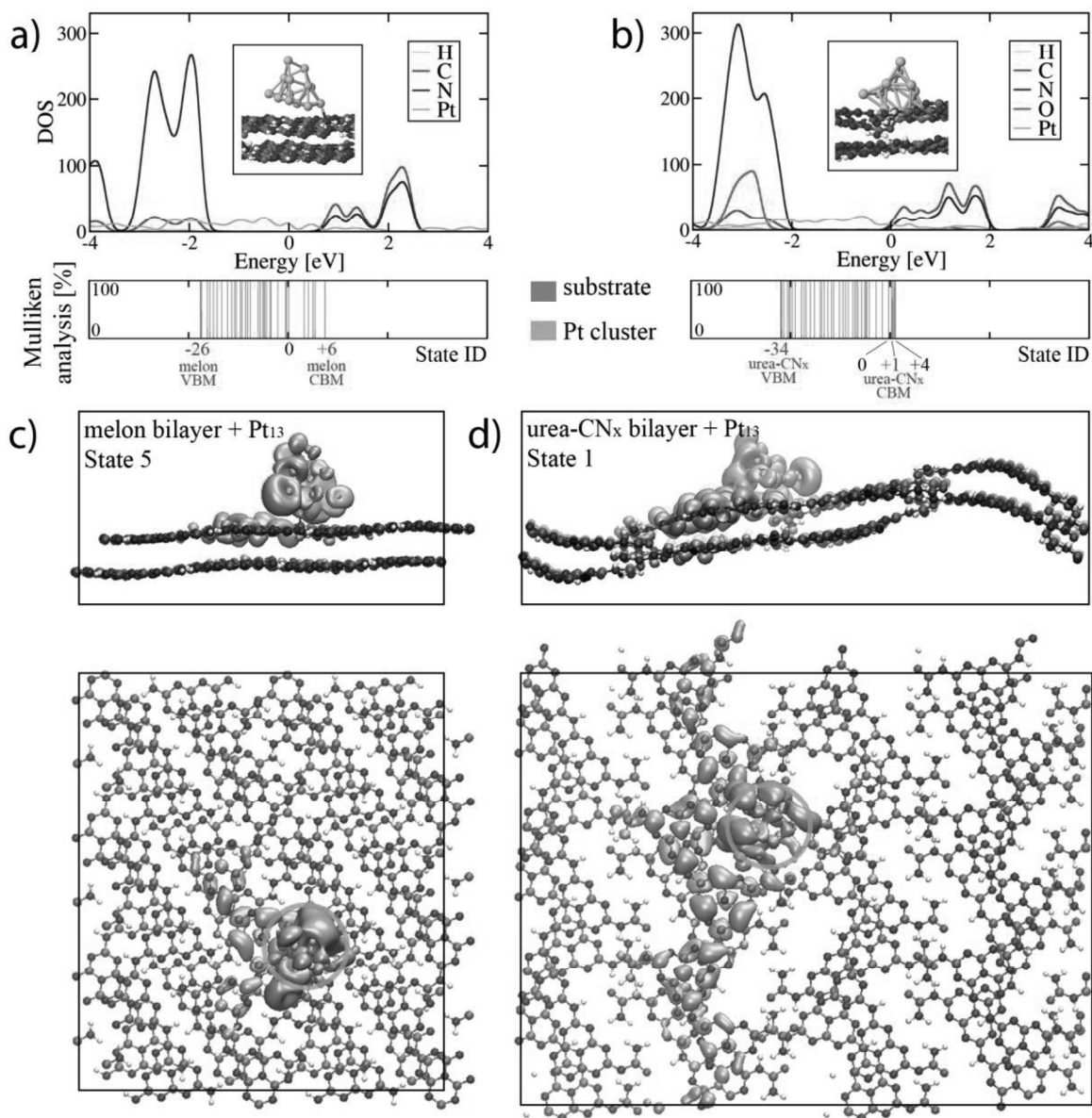


Figure 7. First-principles model of the interaction of melon versus urea-CN_x with a Pt₁₃ cluster. H: white; C: grey; N: blue; O: red; Pt: silver. a) Element-resolved smoothed partial density of states of the melon bilayer + Pt₁₃ cluster model. Inset: Pt₁₃ attachment via NH₂ side group. b) Element-resolved smoothed partial density of states of the urea-CN_x bilayer + Pt₁₃ cluster model used in this work. Inset: Pt₁₃ attachment via O. The lower panels in a) and b) show Mulliken decompositions of selected individual levels inside the melon / urea-CN_x model HOMO-LUMO gaps. Two-colored bars, grey and orange, mark the bilayer substrate vs. Pt₁₃ cluster fractions of each state. Numbers on the x axes index the selected states in order of their single-particle energy, with zero indicating the highest state with a fractional occupation of 0.5 or above. c) Side and top views of the orbital density of the partially hybridized state (state ID 5 in lower panel of a) located at 0.20 eV below the LUMO of the melon substrate (state ID 6 in lower panel of a). d) Top and side views of the orbital density of the strongly hybridized state (state ID 1 in lower panel of b) with contributions from Pt₁₃ and from the urea-CN_x substrate LUMO. Orange rings in the top views indicate the location of the Pt₁₃ cluster.

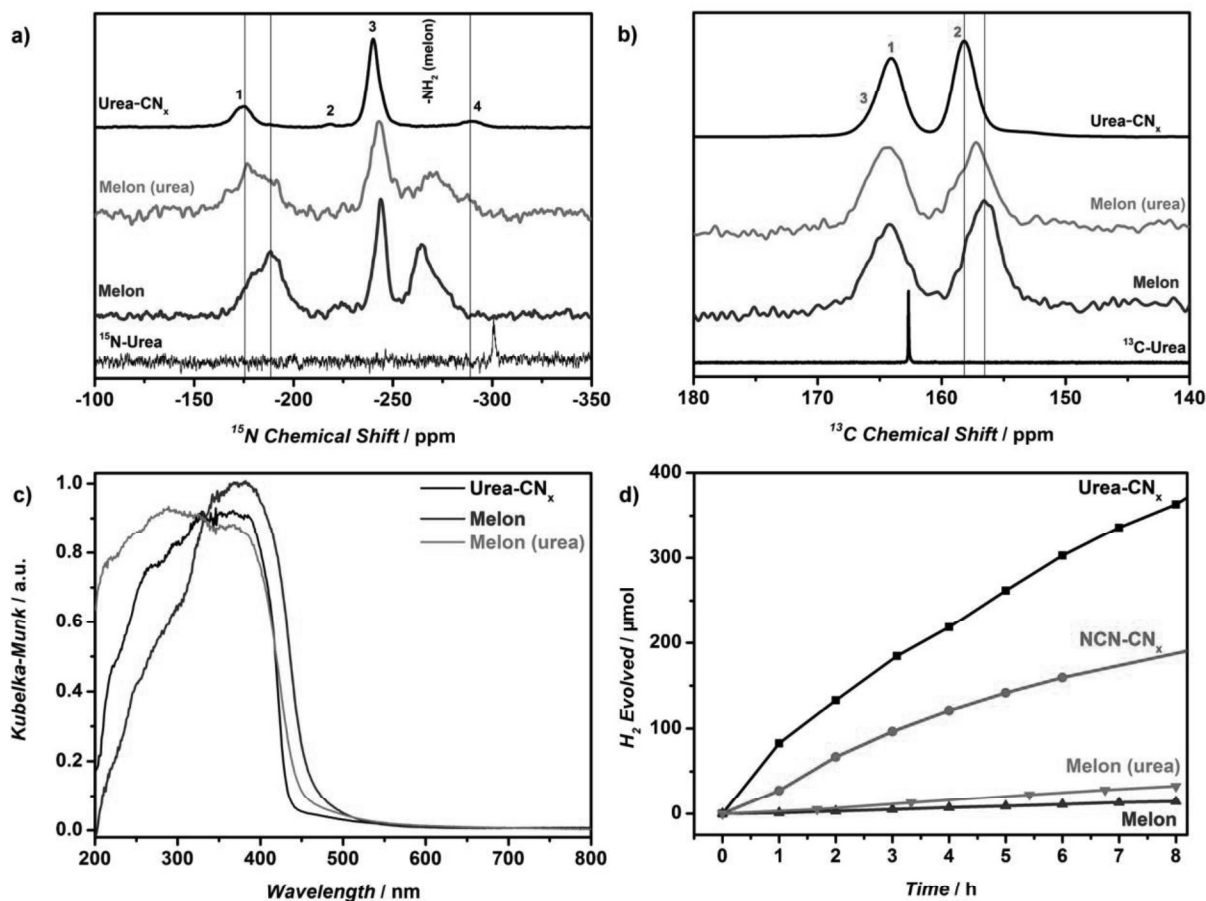


Figure 8. Comparison of urea- CN_x and melon prepared from urea and melamine: a) ^{15}N CP and b) and ^{13}C direct excitation NMR, with lines drawn to illustrate how the spectra for melon (urea) resemble urea- CN_x as compared to melon. Identical to Figure 2c and d, the black and red numbers are assignment of the ^{15}N and ^{13}C signals, respectively, to the proposed local structure of urea- CN_x (Figure 2d inset). Note that both melon and melon (urea) are not isotope-enriched. c) diffuse reflectance UV-Vis spectra, and d) photocatalytic hydrogen evolution from methanol solution and AM1.5 irradiation (right).

Table 1. Elemental analyses and C:N molar ratios of the urea- CN_x , NCN- CN_x , melon, and PHI; all values are weight percentages and uncertainties are the standard deviations of measurement replicates.

	C	N	K	S	C:N molar ratio	C:N molar ratio (th.)
Urea- CN_x	28.8 ± 0.3	48.2 ± 0.2	0.134 ± 0.001	0.017 ± 0.004	0.699 ± 0.007	0.700
NCN- CN_x	26.7 ± 0.0	44.4 ± 0.1	7.54 ± 0.08	0.17 ± 0.11	0.701 ± 0.002	0.700
Melon	35.4 ± 0.1	60.6 ± 0.5	a)	a)	0.681 ± 0.006	0.667^b
PHI ^c	37.4	61.8	-	-	-	0.706

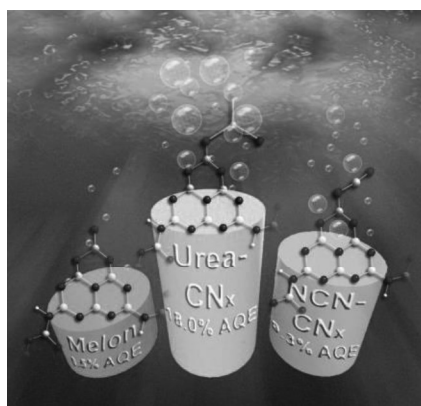
a) Not measured; b) assuming infinite 1D heptazine polymer with a unit cell formula $\text{C}_6\text{N}_9\text{H}_3$; c) Theoretical values based on a unit cell formula of $\text{C}_{12}\text{N}_{17}\text{H}_3$ based on ref 12, but without the central melamine

1 **Defective design:** Graphitic carbon nitride was modified with the urea moiety as a
2 photocatalytically relevant “defect”, yielding a material with a sacrificial photocatalytic
3 hydrogen evolution rate well over an order of magnitude higher than that of the unmodified
4 counterpart. The outperformance is attributed to metal-support interaction between the urea
5 group and the Pt co-catalyst, thereby facilitating interfacial electron transfer.
6

7 **Keyword: Photocatalysis**
8

9
10 Vincent Wing-hei Lau, Victor Wen-zhe Yu, Florian Ehrat, Tiago Botari, Igor Moudrakovski,
11 Thomas Simon, Viola Duppel, Elise Medina, Jacek Stolarczyk, Jochen Feldmann, Volker
12 Blum, and Bettina V. Lotsch*
13

14 **Urea-modified carbon nitrides: Enhancing Photocatalytic Hydrogen Evolution by**
15 **Rational Defect Engineering**
16



Supporting Information

Urea-modified carbon nitrides: Enhancing Photocatalytic Hydrogen Evolution by Rational Defect Engineering

Vincent Wing-hei Lau, Victor Wen-zhe Yu, Florian Ehrat, Tiago Botari, Igor Moudrakovski, Thomas Simon, Viola Duppel, Elise Medina, Jacek Stolarczyk, Jochen Feldmann, Volker Blum, and Bettina V. Lotsch

Experimental details

All chemicals used are reagent grade purity. Melon and NCN-CN_x were prepared following published procedures. Briefly, melon was prepared by heating melamine (14 g) unless otherwise stated, loaded in a lidded quartz boat, in a tube furnace under argon at 550 °C at 5 °C min⁻¹ for 12 h. After cooling to ambient temperature, the yellow solid obtained was thoroughly ground in a ceramic mortar and pestle prior to further processing and analysis (yield 6–7 g). NCN-CN_x was prepared in a salt melt of KSCN as follows. Melon (1.5 g) was thoroughly mixed in a ceramic mortar and pestle with KSCN (3.0 g, dried overnight at 140 °C in vacuum) and the resulting mixture was loaded in an alumina boat. The mixture was then heated in a tube furnace under argon to 400 °C for 1 h, then at 500 °C for 30 min, both at maximum ramp. After cooling to ambient temperature, the product was washed repeatedly with water until all residue of KSCN was removed as judged by XRD, then dried at 60 °C in a vacuum oven, yielding 1.3 g of the product as a yellow solid. Urea-CN_x was prepared by adding aqueous HCl (50 mL, 1 M) to NCN-CN_x (600 mg), whereupon the yellow solid immediately turned off-white. After several hours of stirring, the solid was isolated by centrifugation, washed repeatedly with water, then dried at 60 °C in vacuum. Batch to batch variation of photocatalytic activity is shown in Figure S1.

Melon (urea) was prepared by heating urea (19.4 g) in a lidded quartz boat in a tube furnace under argon flow at 550 °C at 5 °C h⁻¹ ramp for 12 h. The color of the product is pale yellow with yield of 4–5 g.

Instrumental details

X-ray diffraction patterns were collected using a STOE Stadi P diffractometer (Cu K α 1) in Debye-Scherrer configuration. ATR-IR spectra were collected with a PerkinElmer UATR TWO spectrometer equipped with a diamond crystal. Diffuse reflectance UV-Vis spectra were collected on a Cary 5000 spectrometer (referenced to PTFE or barium sulfate) and the

1 spectra in percentage reflectance were converted using the Kubelka Munk function. From
2 these spectra, the optical gaps were extracted assuming direct transition.
3

4 CHN elemental analyses were performed with a Vario El element analyzer (Elementar
5 Analysensysteme GmbH). Other elements were quantified with a Vista Pro Simultaneous
6 ICP-OES Spectrometer combined with axially plasma system as excitation source and echelle
7 polychromator with CCD detector (Varian Darmstadt). Calibrations were carried out by
8 standard addition and the data were analyzed by the ICP-Expert software. Samples were
9 digested in concentrated HNO₃ at 150 °C for 14 h in a Teflon-lined autoclave.
10
11

12 Liquid state ¹H, ¹³C and ¹⁵N NMR spectra were collected on a Bruker Avance 300 MHz
13 NMR spectrometer at resonance frequencies of 300, 75.5 and 30.4 MHz, respectively (B₀ =
14 7.04 T). Solid-state ¹H, ¹³C and ¹⁵N NMR experiments were performed on a Bruker Avance-
15 III 400 MHz instrument at the frequencies of 400, 100.61 and 40.53 MHz, respectively (B₀ =
16 9.4 T). Chemical shifts for ¹H and ¹³C are referenced to tetramethylsilane (TMS, δ(¹H,¹³C) =
17 0.0 ppm), while ¹⁵N is referenced to nitromethane (δ = 0.0 ppm, with positive shifts to higher
18 frequency). Magic Angle Spinning (MAS) with spinning rates ranging between 10 and 12.5
19 kHz was used in all experiments on solids. ¹³C spectra with cross-polarization (CP) were
20 recorded with a ramped polarization mixing and SPINAL-64 proton decoupling (¹H RF field
21 of 80 kHz).^[1] Quantitative ¹³C spectra were acquired in a direct excitation mode with
22 relaxation delay between the consecutive scans set to 900 s. This relaxation delay was at least
23 4 times the longest T₁ in all carbon sites in the materials studied, as estimated from
24 preliminary relaxation time measurements. Between 160 and 256 scans were commonly
25 accumulated, with all experiments accompanied by SPINAL-64 decoupling. ¹H-¹³C and ¹H-
26 ¹⁵N frequency switched Lee-Goldburg hetero-nuclear correlations (FSLG HETCOR)
27 experiments^[2] were carried out with ramped cross polarization, ¹H RF =100 kHz, and
28 spinning speed of 12.5 kHz. Short mixing times of 50 -150 μs were used in order to avoid
29
30
31
32
33
34
35
36
37
38
39
40
41
42
43
44
45
46
47
48
49
50
51
52
53
54
55
56
57
58
59
60
61
62
63
64
65

1 long range polarization transfer. A total of 128 increments were made in an indirect
2 dimension (^1H), with 560 acquisitions per increment. Deconvolution and integration of the
3
4 solid state spectra were carried out using the *Dmfit* software version 20111221.^[3] A Cross-
5
6 Polarization with Polarization Inversion (CPPI) experiment implemented previously reported
7
8 pulse sequences.^[4] A ramped mixing pulse of 5 ms was followed by a proton polarization
9
10 inverting pulse in a range of 10 to 500 μs . In Double Cross-Polarizations (DCP)
11
12 experiments^[5] the first CP step transfers magnetization from protons to ^{15}N . Then, in a second
13
14 cross polarization step, magnetization is transferred from ^{15}N to ^{13}C . The signal is detected on
15
16 ^{13}C under SPINAL-64 proton decoupling. Ramped and tangential mixing pulses were used in
17
18 the consecutive cross-polarization steps with optimized durations of 0.4-0.6 ms and 9 ms. A
19
20 total of 128 increments were made in an indirect dimension (^{15}N), with 192 acquisitions per
21
22 increment and a relaxation delay of 2s.
23
24
25
26
27

28 Sorption measurements were performed on a Quantachrome Autosorb iQ gas sorption
29
30 analyzer using argon as the sorbent at 87.45 K. Samples were outgassed for overnight at
31
32 150 °C to a vacuum of 10^{-7} mbar. Surface areas were calculated using Brunauer–Emmett–
33
34 Teller (BET) theory from the argon adsorption isotherms of the samples. Pore size
35
36 distribution and volume were calculated from the adsorption isotherm employing either the
37
38 non-local (NLDFT) or quenched solid density functional theory (QSDFT) using the “Ar-
39
40 Carbon cylindrical pores at 87 K” or the “Ar-Carbon slit pores at 87 K” kernel (applicable
41
42 pore diameters 0.35 – 36 nm) as implemented in the AUTOSORB data reduction software.
43
44
45
46
47

48 Transmission electron microscopy (TEM) was performed with a Philips CM30 ST (300 kV,
49
50 LaB6 cathode). The samples were suspended in n-butanol and drop-cast onto a lacey carbon
51
52 film (Plano). Scanning electron microscopy (SEM) was performed on a Zeiss Merlin electron
53
54 microscope.
55
56
57
58
59
60
61
62
63
64
65

1 For X-ray photoelectron spectroscopy (XPS), samples were pressed onto indium foil and the
2 spectra were collected on an Axis Ultra (Kratos Analytical, Manchester) X-ray photoelectron
3 spectrometer with charge neutralization. The spectra were processed using the software
4 CasaXPS 2.3.16. The spectra were referenced with the adventitious carbon 1s peak at
5 284.80 eV. Binding energies were compared with the NIST Standard Reference Database 20
6 (Version 4.1) unless otherwise specified.
7

8
9
10
11
12
13
14 Thermogravimetric analysis coupled with mass spectroscopy (TGA-MS) was performed with
15 the instrument STA 409 C (Netzsch GmbH, Selb, Germany) connected with a quadrupole
16 mass spectrometer QMS 422 (Balzers, Hudson, USA). Samples were loaded in alumina
17 crucibles and heated under argon (100 mL min^{-1}) from ambient temperature to $900 \text{ }^\circ\text{C}$ at a
18 ramp rate of $1 \text{ }^\circ\text{C min}^{-1}$.
19

20
21
22
23
24
25
26 Static photoluminescence (PL) spectra were acquired with a Horiba Jobin Yvon Fluorolog-3
27 FL3-22 spectrometer equipped with a water-cooled Horiba R928 PMT detector. Fluorescence
28 was detected at an angle of 160° with respect to the excitation source. The samples were
29 measured at a suspension concentration of 1 mg mL^{-1} in water or aqueous methanol solution
30 (10 vol%). The suspension was stirred during the measurement to prevent suspension
31 sedimentation.
32

33
34
35
36
37
38
39
40
41 Time resolved fluorescence measurements were carried out with a TCSPC setup. A
42 NKT SuperK white light laser with ExtendUV was used as the excitation source at 375 nm.
43
44
45
46
47
48
49
50
51
52
53
54
55
56
57
58
59
60
61
62
63
64
65

66
67
68
69
70
71
72
73
74
75
76
77
78
79
80
81
82
83
84
85
86
87
88
89
90
91
92
93
94
95
96
97
98
99
100
101
102
103
104
105
106
107
108
109
110
111
112
113
114
115
116
117
118
119
120
121
122
123
124
125
126
127
128
129
130
131
132
133
134
135
136
137
138
139
140
141
142
143
144
145
146
147
148
149
150
151
152
153
154
155
156
157
158
159
160
161
162
163
164
165
166
167
168
169
170
171
172
173
174
175
176
177
178
179
180
181
182
183
184
185
186
187
188
189
190
191
192
193
194
195
196
197
198
199
200
201
202
203
204
205
206
207
208
209
210
211
212
213
214
215
216
217
218
219
220
221
222
223
224
225
226
227
228
229
230
231
232
233
234
235
236
237
238
239
240
241
242
243
244
245
246
247
248
249
250
251
252
253
254
255
256
257
258
259
260
261
262
263
264
265
266
267
268
269
270
271
272
273
274
275
276
277
278
279
280
281
282
283
284
285
286
287
288
289
290
291
292
293
294
295
296
297
298
299
300
301
302
303
304
305
306
307
308
309
310
311
312
313
314
315
316
317
318
319
320
321
322
323
324
325
326
327
328
329
330
331
332
333
334
335
336
337
338
339
340
341
342
343
344
345
346
347
348
349
350
351
352
353
354
355
356
357
358
359
360
361
362
363
364
365
366
367
368
369
370
371
372
373
374
375
376
377
378
379
380
381
382
383
384
385
386
387
388
389
390
391
392
393
394
395
396
397
398
399
400
401
402
403
404
405
406
407
408
409
410
411
412
413
414
415
416
417
418
419
420
421
422
423
424
425
426
427
428
429
430
431
432
433
434
435
436
437
438
439
440
441
442
443
444
445
446
447
448
449
450
451
452
453
454
455
456
457
458
459
460
461
462
463
464
465
466
467
468
469
470
471
472
473
474
475
476
477
478
479
480
481
482
483
484
485
486
487
488
489
490
491
492
493
494
495
496
497
498
499
500
501
502
503
504
505
506
507
508
509
510
511
512
513
514
515
516
517
518
519
520
521
522
523
524
525
526
527
528
529
530
531
532
533
534
535
536
537
538
539
540
541
542
543
544
545
546
547
548
549
550
551
552
553
554
555
556
557
558
559
560
561
562
563
564
565
566
567
568
569
570
571
572
573
574
575
576
577
578
579
580
581
582
583
584
585
586
587
588
589
590
591
592
593
594
595
596
597
598
599
600
601
602
603
604
605
606
607
608
609
610
611
612
613
614
615
616
617
618
619
620
621
622
623
624
625
626
627
628
629
630
631
632
633
634
635
636
637
638
639
640
641
642
643
644
645
646
647
648
649
650
651
652
653
654
655
656
657
658
659
660
661
662
663
664
665
666
667
668
669
670
671
672
673
674
675
676
677
678
679
680
681
682
683
684
685
686
687
688
689
690
691
692
693
694
695
696
697
698
699
700
701
702
703
704
705
706
707
708
709
710
711
712
713
714
715
716
717
718
719
720
721
722
723
724
725
726
727
728
729
730
731
732
733
734
735
736
737
738
739
740
741
742
743
744
745
746
747
748
749
750
751
752
753
754
755
756
757
758
759
760
761
762
763
764
765
766
767
768
769
770
771
772
773
774
775
776
777
778
779
780
781
782
783
784
785
786
787
788
789
790
791
792
793
794
795
796
797
798
799
800
801
802
803
804
805
806
807
808
809
810
811
812
813
814
815
816
817
818
819
820
821
822
823
824
825
826
827
828
829
830
831
832
833
834
835
836
837
838
839
840
841
842
843
844
845
846
847
848
849
850
851
852
853
854
855
856
857
858
859
860
861
862
863
864
865
866
867
868
869
870
871
872
873
874
875
876
877
878
879
880
881
882
883
884
885
886
887
888
889
890
891
892
893
894
895
896
897
898
899
900
901
902
903
904
905
906
907
908
909
910
911
912
913
914
915
916
917
918
919
920
921
922
923
924
925
926
927
928
929
930
931
932
933
934
935
936
937
938
939
940
941
942
943
944
945
946
947
948
949
950
951
952
953
954
955
956
957
958
959
960
961
962
963
964
965
966
967
968
969
970
971
972
973
974
975
976
977
978
979
980
981
982
983
984
985
986
987
988
989
990
991
992
993
994
995
996
997
998
999
1000

1 NaOH, with the ionic strength maintained at 10 mM using NaCl. The suspension was
2 sonicated for 15 min before loading in a folded capillary cell (Malvern) for measurement.
3

4 **Photocatalytic experiments**

5
6
7 Photocatalytic experiments were performed in a double-walled glass reactor, where the outer
8 compartment is circulated with thermostated water (25 °C), as previously described.^[6] In the
9
10 platinum-free cases, the reactor and magnetic stirrer were cleaned with aqua regia prior to the
11
12 photocatalysis experiment. The reactor was top-irradiated through a quartz window with a
13
14 xenon lamp (Newport, 300 W) equipped with a water filter and a full spectrum mirror
15
16 (2000 nm > λ > 200 nm). An air mass (AM) 1.5 filter was also used where specified. Unless
17
18 stated otherwise, for a standard photocatalytic experiment, the catalyst powder (20 mg) was
19
20 suspended in a solution of water (18 mL), methanol (2 mL) and dihydrogen
21
22 hexachloroplatinate (5 μ L, 8 wt% aqueous solution, Aldrich), which forms the platinum
23
24 cocatalyst from its *in-situ* reduction. This platinum amount yields a loading of around 1 wt%.
25
26
27 The photocatalytic experiments in pure water followed an identical procedure, except that
28
29 only water (20 mL) was used (i.e. no methanol nor dihydrogen hexachloroplatinate). The
30
31 headspace was subjected to several cycles of evacuation and argon backfill prior to the
32
33 experiment. In the course of the experiment, the headspace of the reactor was periodically
34
35 sampled and hydrogen was quantified by gas chromatography (Thermo Scientific TRACE
36
37 GC Ultra) equipped with a TCD detector using argon as the carrier gas.
38
39

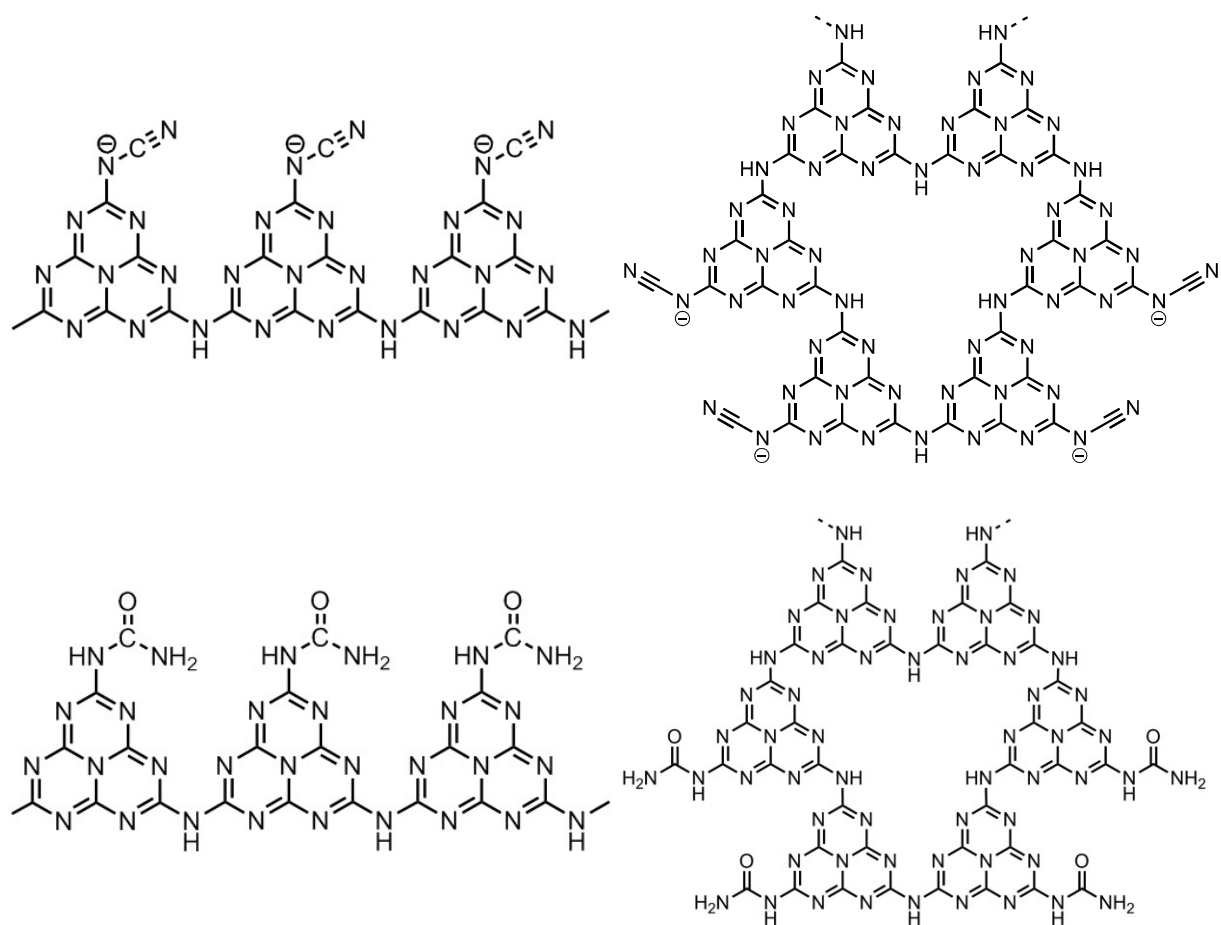
40
41
42 After the photocatalytic experiment, the catalyst was recovered by centrifugation, washed
43
44 with water, then dried at 60 °C in vacuum. For quick optimization of platinum loading, the
45
46 photocatalytic experiments were performed in disposable septum-capped glass vials
47
48 containing the catalyst (10 mg), water (9 mL) and methanol (1 mL) and a variable amount of
49
50 dihydrogen hexachloroplatinate solution. The vial was stirred whilst irradiated using a xenon
51
52 lamp as above for 3 h, then the hydrogen in the headspace was quantified. Experiments for
53
54
55
56
57
58
59
60
61
62
63
64
65

1 the estimation of quantum efficiency were conducted using band pass filters with band
2 centers at 400 nm and 500 nm with full width half maximum of 50 nm (Thorlab). Irradiance
3 of the incident light was measured using a thermopile (Thorlabs) and photon flux was
4 estimated using the integral of the transmission spectra of the band pass filters. Apparent
5 quantum efficiency (AQE) was then calculated as:
6
7
8
9
10

$$11 \quad AQE [\%] = \frac{2 \times \textit{Hydrogen Evolution Rate} [\textit{mol h}^{-1}]}{12 \quad \textit{Photon Flux} [\textit{mol h}^{-1}]}$$

13
14
15
16
17 Further details of our photocatalytic experiments (e.g. schematic of our set-up, reactor
18 configuration, spectra of our irradiation sources) can be found in our previous publication.^[6]
19
20
21
22
23
24
25
26
27
28
29
30
31
32
33
34
35
36
37
38
39
40
41
42
43
44
45
46
47
48
49
50
51
52
53
54
55
56
57
58
59
60
61
62
63
64
65

Alternative structures of NCN-CN_x and urea-CN_x



Scheme S1 Structures of NCN-CN_x (top row) and urea-CN_x (bottom row) based on the 1D polymeric structure (left column) and the PHI network structure (right column).

Characterization of urea-CN_x and other carbon nitrides

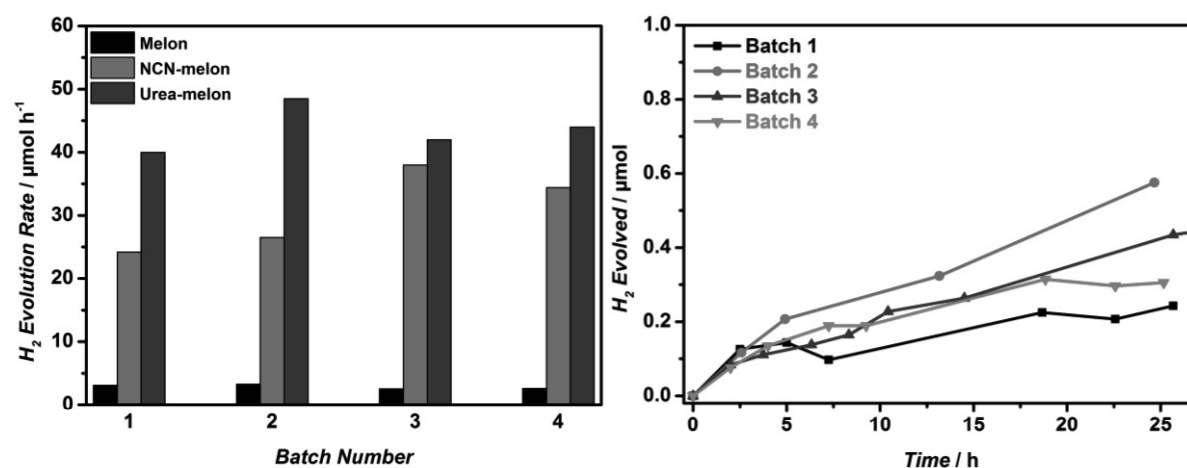


Figure S1 Variation of photocatalytic activity of four batches of catalysts under AM1.5 irradiation and methanol (10 vol%) as electron donor. Left: initial photocatalytic hydrogen evolution (average rate of first six hours) for the carbon nitrides at optimized platinum loading. Right: platinum-free hydrogen evolution of urea-CN_x for the first 25 h.

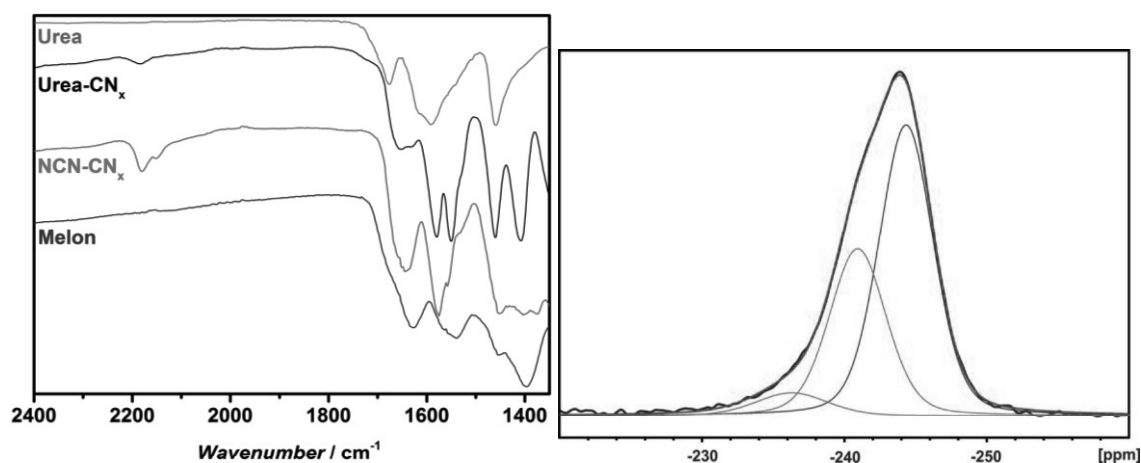


Figure S2 Left: enlarged version of the FTIR spectra in Figure 2a, focusing on the cyanamide (2300–2100 cm⁻¹) and urea region (1800–1400 cm⁻¹). Right: deconvolution of the N₃ signal from the ¹⁵N CP spectrum of urea-CN_x.

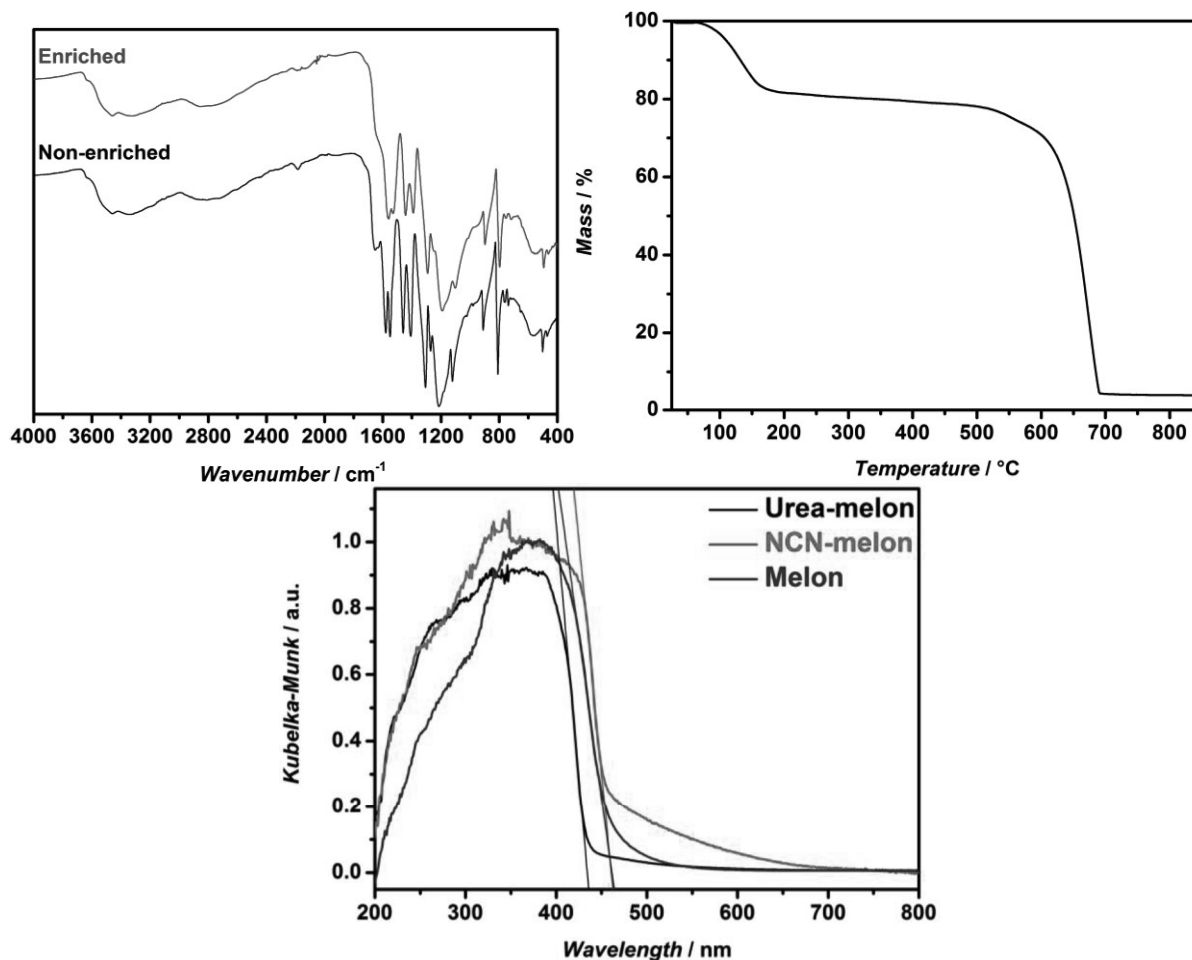


Figure S3 Top left: comparison of the FTIR spectra of urea-CN_x of natural isotope abundance and the sample prepared from ¹³C and ¹⁵N enriched KSCN; top right: thermogravimetric analysis of urea-CN_x; bottom: diffuse reflectance spectra and extraction of their optical gaps.

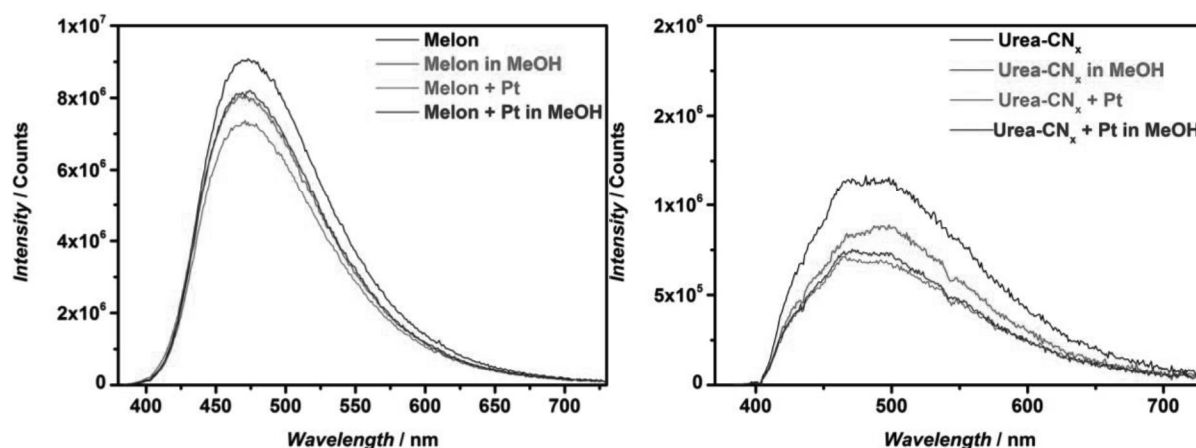


Figure S4 Steady state PL spectra of melon (left) and urea-CN_x (right).

1
2
3
4
5
6
7
8
9
10
11
12
13
14
15
16
17
18
19
20
21
22
23
24
25
26
27
28
29
30
31
32
33
34
35
36
37
38
39
40
41
42
43
44
45
46
47
48
49
50
51
52
53
54
55
56
57
58
59
60
61
62
63
64
65

Table S1 Elemental analyses of urea-CN_x before and after 100+ h photocatalysis. All values unless otherwise stated are weight percentages and uncertainties are the standard deviations of the measurement replicates.

	C	N	Pt	C:N molar ratio	Residual Weight (%)
Pristine	28.9 ± 0.3	48.2 ± 0.2	-	0.698 ± 0.007	19.6
Spent	27.9 ± 0.3	45.0 ± 0.1	0.77 ± 0.01	0.724 ± 0.007	21.2

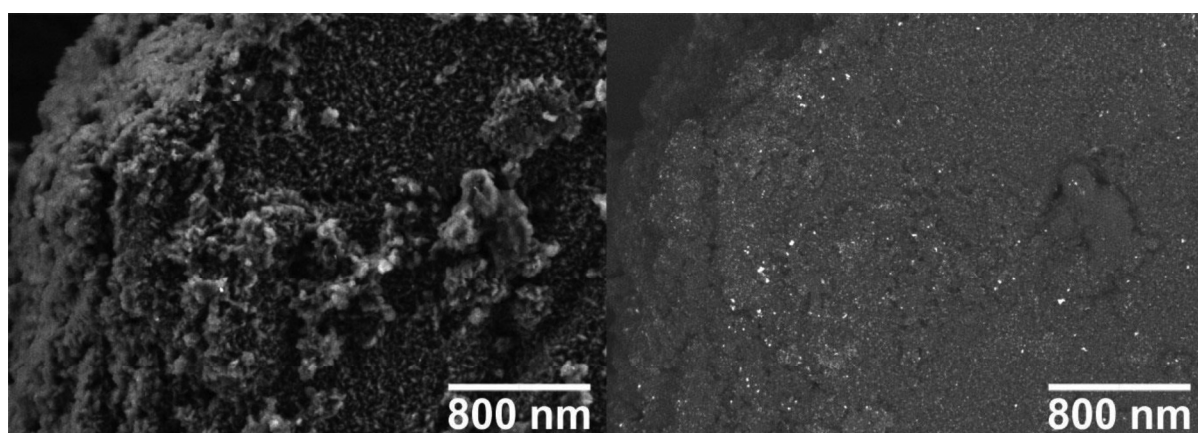


Figure S5 SEM images of the spent urea-CN_x using the secondary electron detector (left) and backscattered electron detector (right), the latter of which shows the platinum particles as bright spots.

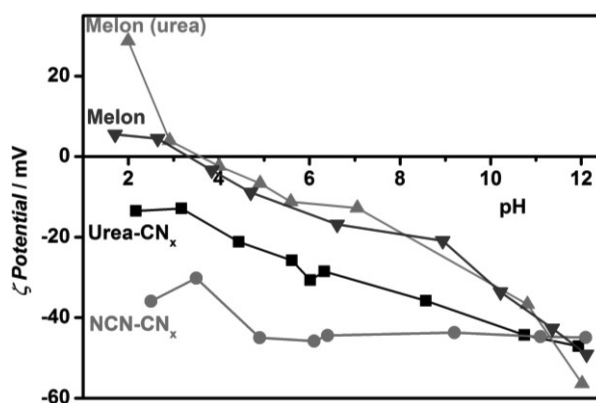


Figure S6 Zeta-potentials of the carbon nitrides studied in this work.

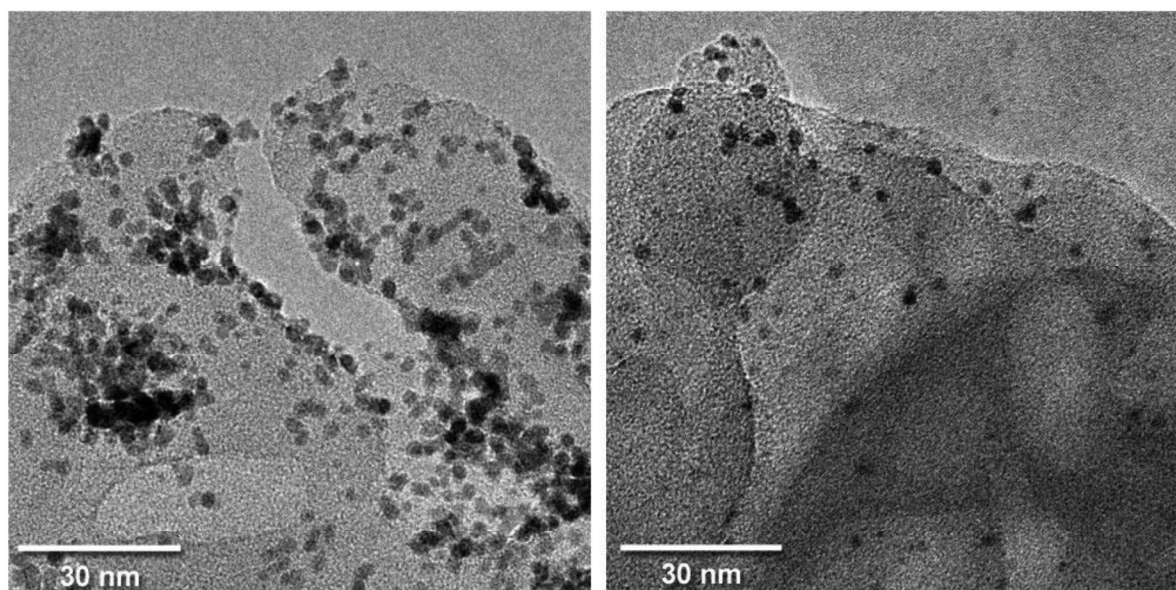


Figure S7 TEM images of melon (left) and melon (urea) (right) after photocatalytic reaction, showing the photo-deposited platinum clusters as dark spots.

By comparing the structure-property-activity relationship in these four carbon nitrides, we can identify the dominant factor leading to high photocatalytic activity in these materials. In agreement with the results from Martin et al,^[7] we can rule out BET surface area based on the differences in their intrinsic activity (hydrogen evolution rate normalized for BET surface area, column 6 in Table S3). Since the hydrogen evolution rate is for illumination under the entire AM1.5 spectrum, the low value for melon (urea) here does not take into account its much higher activity under 400 nm irradiation (*c.f.* AQE values for the four samples). We also rule out water dispersibility as measured by zeta potential (Figure S6) since, at pH \approx 5 where the photocatalytic experiments were performed, the second most active NCN-CN_x has the highest dispersibility due to its anionic charge, while melon (urea) and melon have nearly identical zeta potential despite the former being twice as active as the latter. The most active material, urea-CN_x, has zeta potential in-between NCN-CN_x and the two melon samples. Note that melon is the only sample out of the four that shows significant settling. Zeta potential here thus measures only the melon particles that are sufficiently small (<2 μ m) to maintain colloidal stability.

1 The photo-deposited Pt co-catalyst in all four platinized samples are nearly spherical with
2 diameter in the range of 2–4 nm (Figure S7 for platinized melon and melon (urea); see
3 reference [8] for NCN-CN_x) at loading of below 1 wt% for all but the NCN-CN_x sample
4 (Table S2 for elemental analyses). From the similarity of the Pt size and morphology as well
5 as the absence of correlation between optimized Pt loading and hydrogen evolution rate, we
6 thus rule these out as factors for the activity difference. Lastly, we observed that the Pt
7 particles on urea-CN_x and melon (urea) are distributed over the entire carbon nitride surface,
8 while those of melon suffer from aggregation; note that the apparent aggregation of Pt on
9 NCN-CN_x is due to the much higher optimized Pt loading (5 wt% for NCN-CN_x vs 0.8 wt%
10 for urea-CN_x). The metal–support interaction described in the computational section can
11 rationalize these results as this effect is known to enhance the dispersion of metal
12 nanoparticles as they nucleate,^[9] which we believe to operate for urea-CN_x as well. However,
13 this dispersibility in itself does not explain the order-of-magnitude difference in hydrogen
14 evolution rate between urea-CN_x and melon (urea). Having eliminated these aforementioned
15 factors, we thus deduce efficient charge transfer mediated by the platinum/urea-CN_x
16 interaction to be a key determinant for its high activity. Future work examining this interface
17 in details may clarify the role of such metal–support interaction, and may enable further
18 improvement in the catalyst design process.
19
20
21
22
23
24
25
26
27
28
29
30
31
32
33
34
35
36
37
38
39
40
41
42
43
44
45
46
47
48
49
50
51
52
53
54
55
56
57
58
59
60
61
62
63
64
65

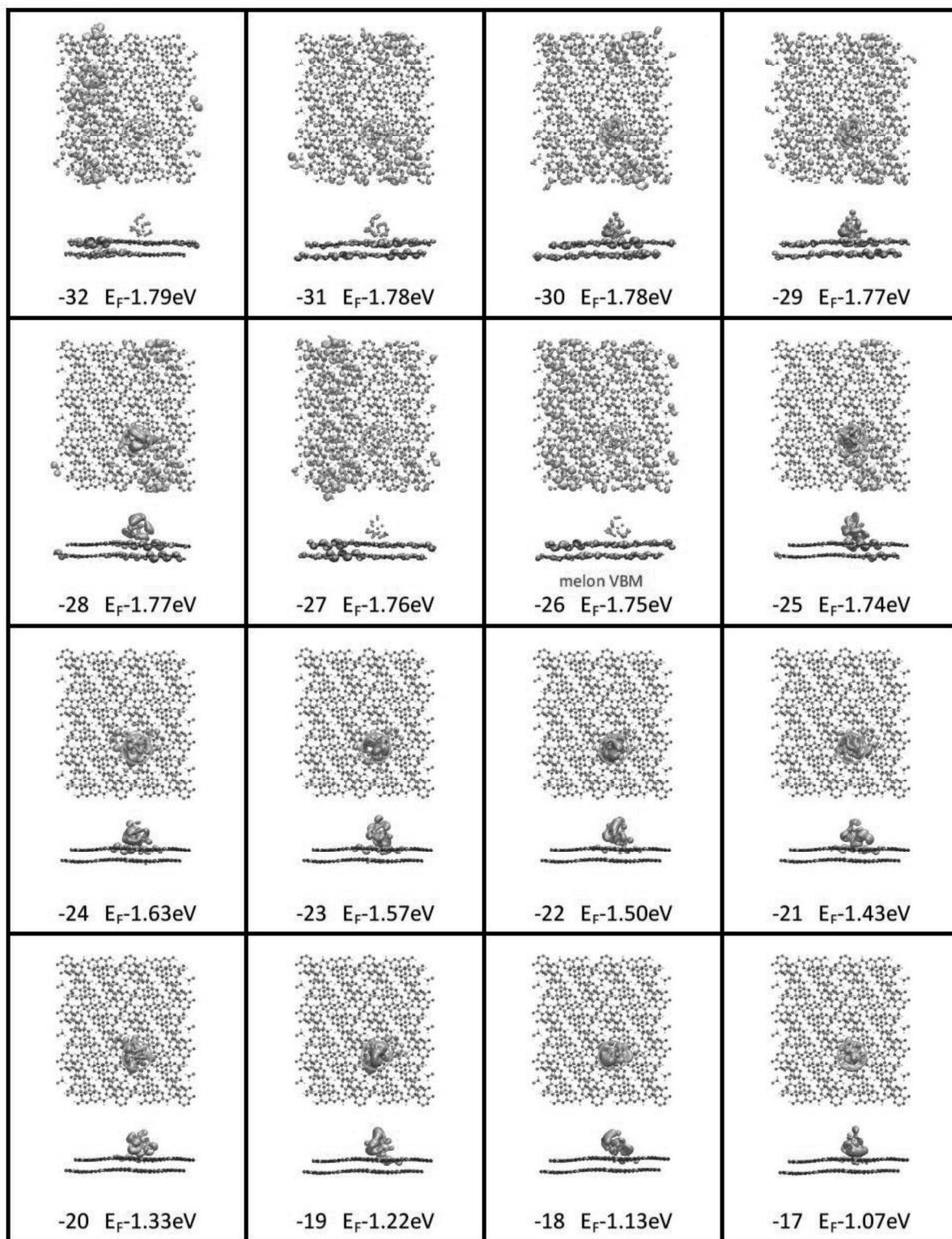


Figure S8 Part 1 of the orbital plots of Pt₁₃-Melon from just below the valence band maximum (VBM) to just above the conduction band minimum (CBM)

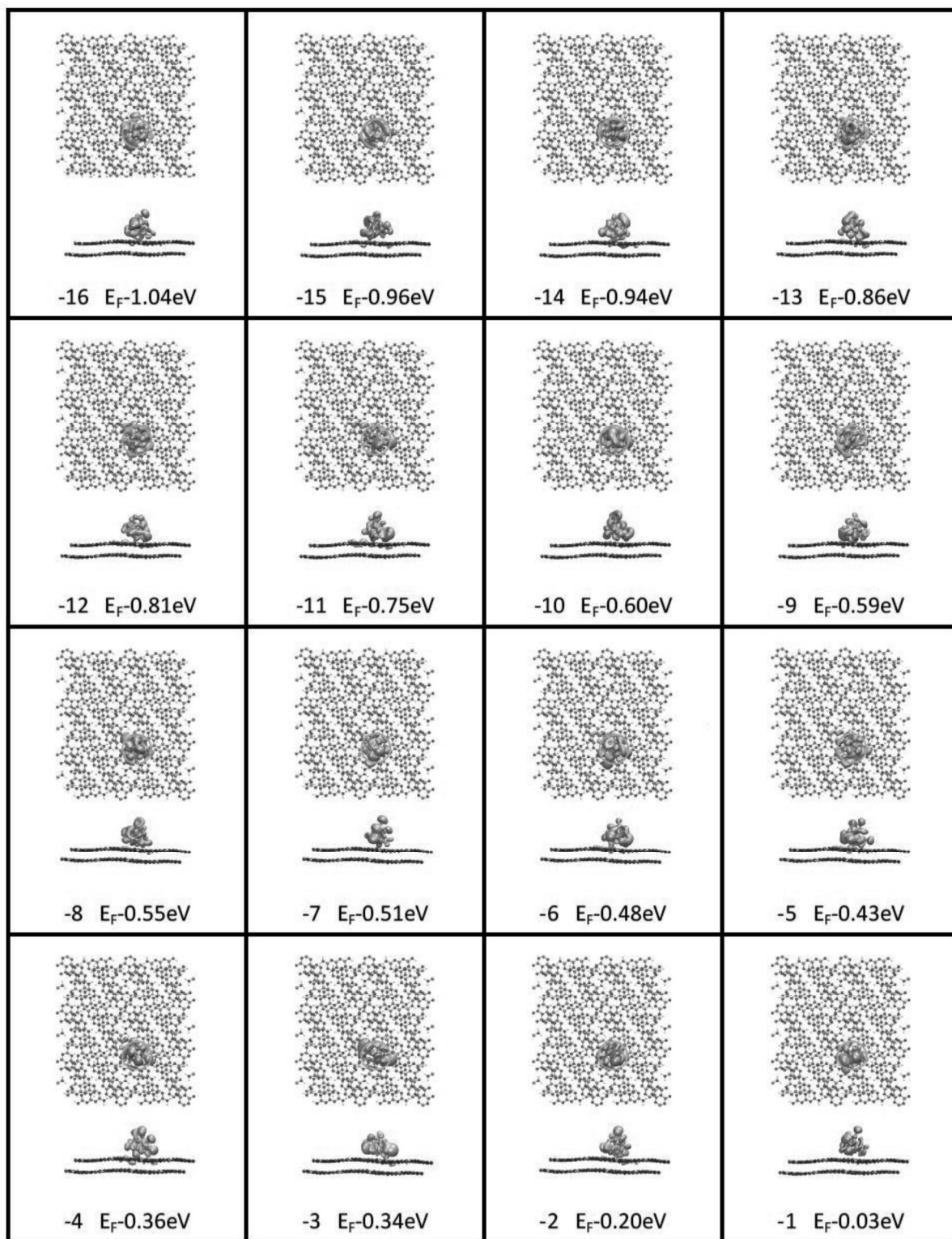


Figure S9 Part 2 of the orbital plots of Pt₁₃-Melon from just below the valence band maximum (VBM) to just above the conduction band minimum (CBM)

1
2
3
4
5
6
7
8
9
10
11
12
13
14
15
16
17
18
19
20
21
22
23
24
25
26
27
28
29
30
31
32
33
34
35
36
37
38
39
40
41
42
43
44
45
46
47
48
49
50
51
52
53
54
55
56
57
58
59
60
61
62
63
64
65

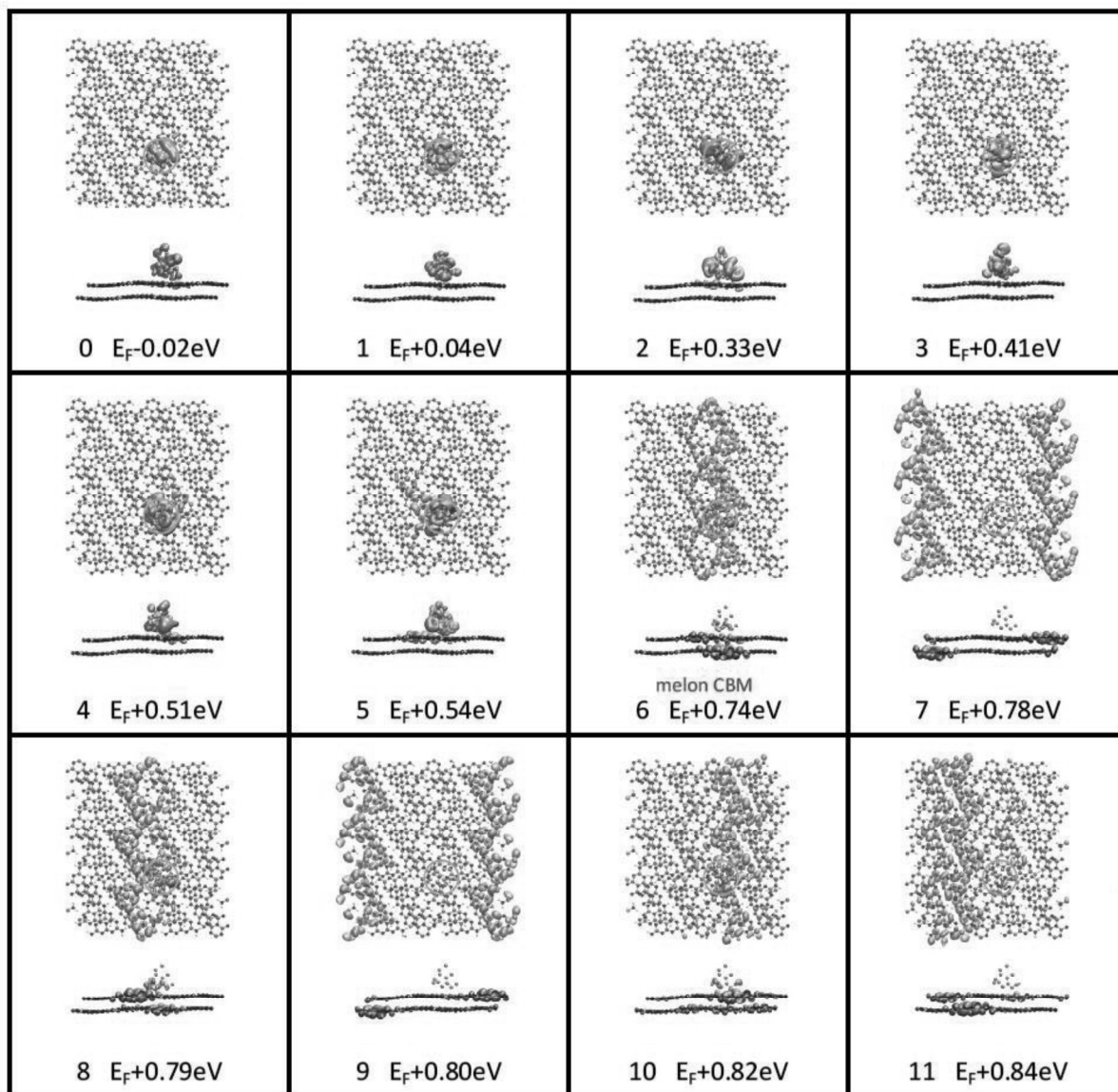


Figure S10 Part 3 of the orbital plots of Pt₁₃-Melon from just below the valence band maximum (VBM) to just above the conduction band minimum (CBM)

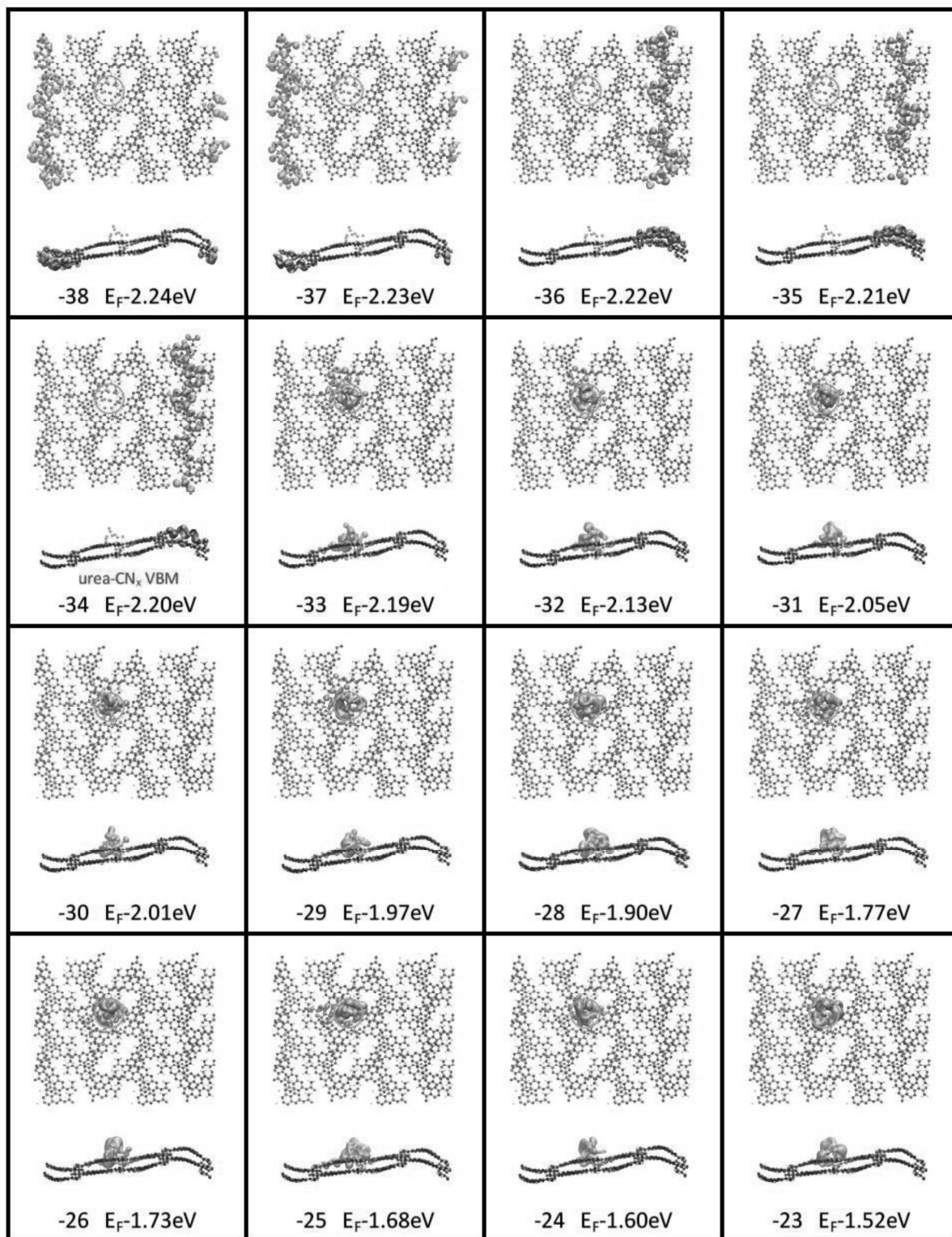


Figure S11 Part 1 of the orbital plots of $\text{Pt}_{13}\text{-urea-CN}_x$ from just below the valence band maximum (VBM) to just above the conduction band minimum (CBM)

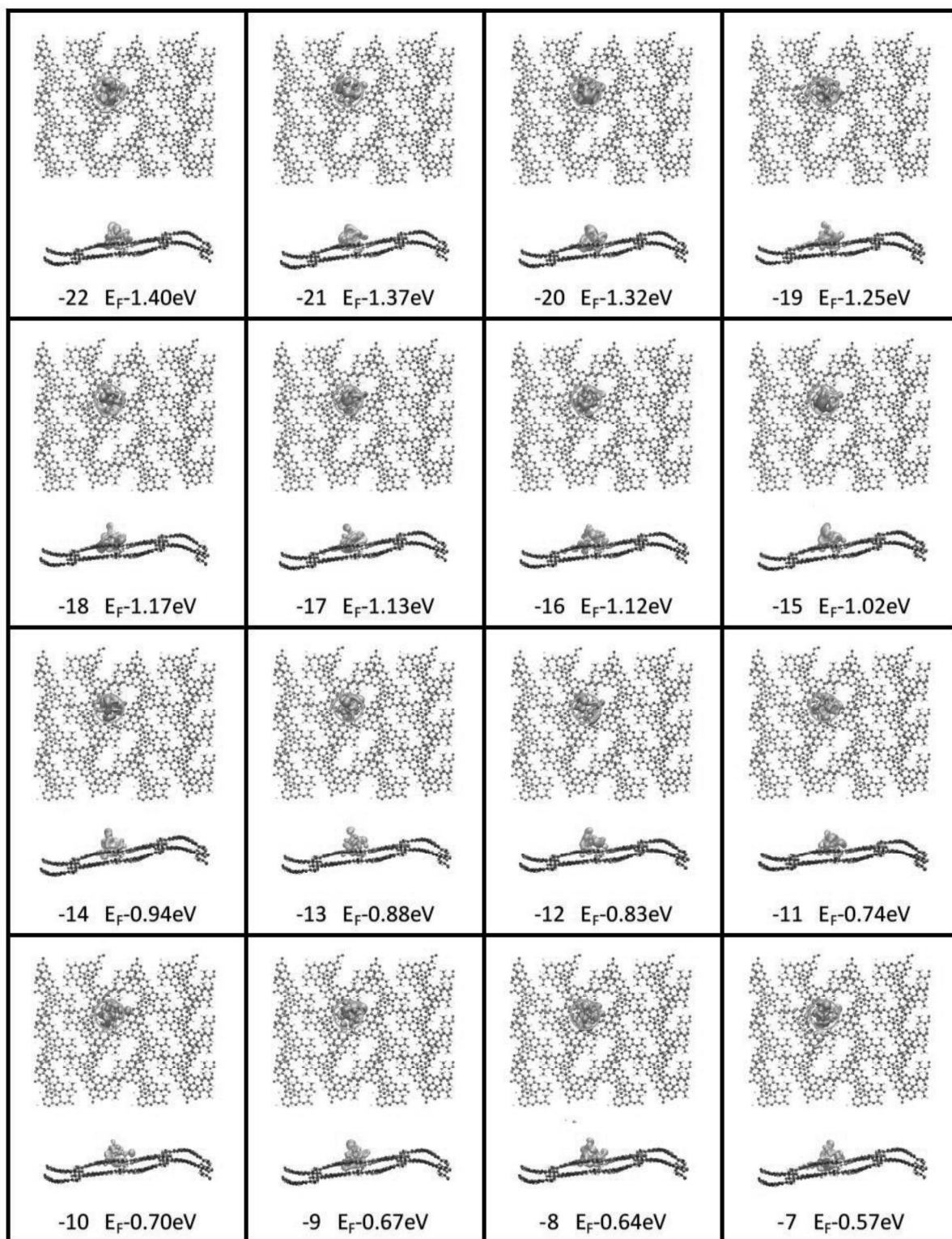


Figure S12 Part 2 of the orbital plots of Pt_{13} -urea- CN_x from just below the valence band maximum (VBM) to just above the conduction band minimum (CBM)

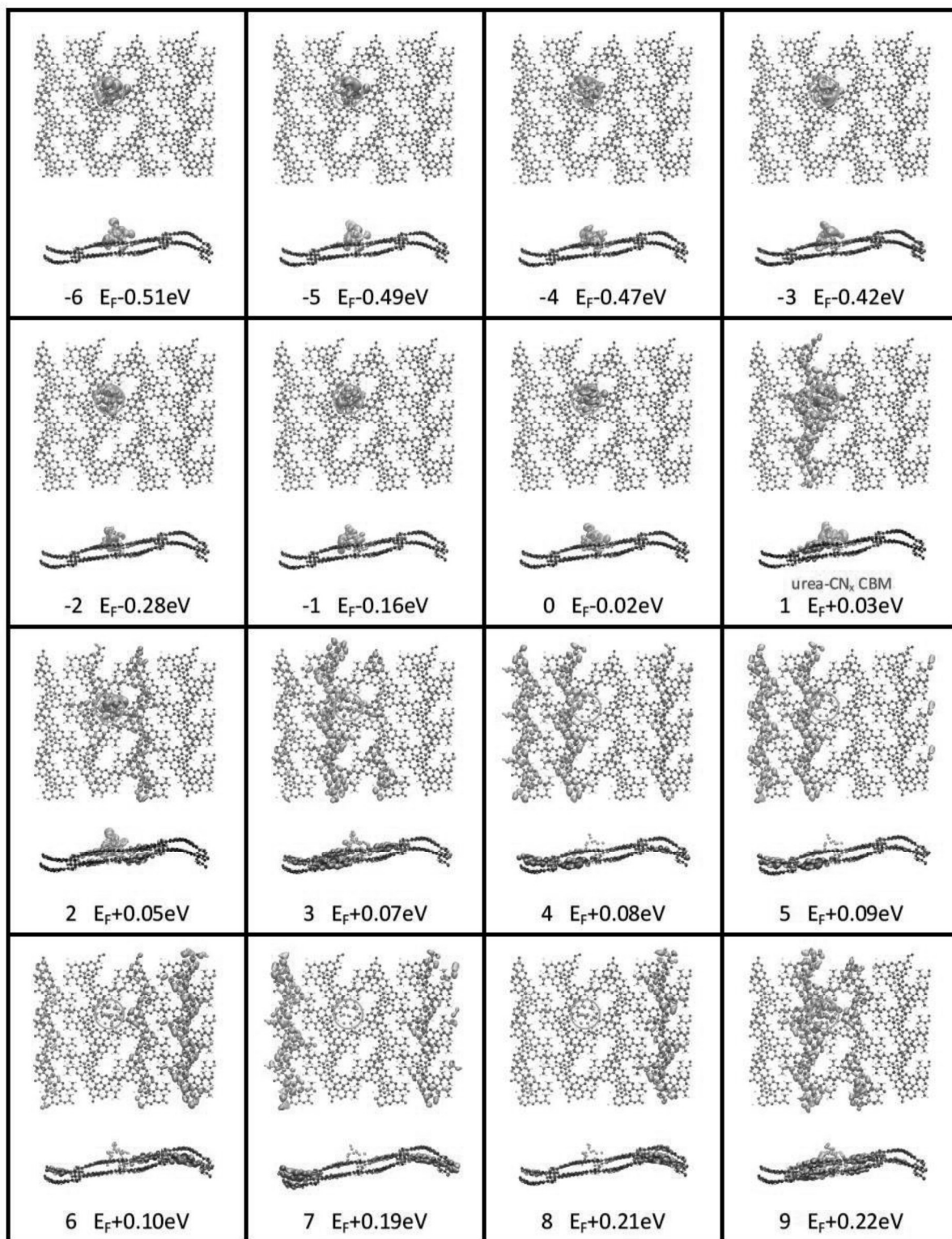


Figure S13 Part 1 of the orbital plots of $\text{Pt}_{13}\text{-urea-CN}_x$ from just below the valence band maximum (VBM) to just above the conduction band minimum (CBM)

15
16
17
18
19
20
21
22
23
24
25
26
27
28
29
30
31
32
33
34
35
36
37
38
39
40
41
42
43
44
45
46
47
48
49
50
51
52
53
54
55
56
57
58
59
60
61
62
63
64
65

Table S2 Elemental analyses in weight percentages of all spent carbon nitrides studied in this work at the platinum loading optimized for hydrogen evolution.

	C	N	Pt	Residual Weight (%)
Urea-CN _x	27.9 ± 0.3	45.0 ± 0.1	0.77 ± 0.01	21.2
NCN-CN _x *	27.6 ± 0.1	43.6 ± 0.1	5.33	23.5
Melon	33.7 ± 0.04	57.2 ± 0.2	0.91 ± 0.04	8.19
Melon (urea)	31.3 ± 0.05	52.5 ± 0.3	0.83 ± 0.01	15.4

*Results from reference [8]

Table S3 Summary of photocatalytic performance metrics and the BET surface areas

	Optical gap (eV)*	H ₂ evolution rate** (μmol h ⁻¹)	Apparent quantum efficiency (%)†	BET surface area (m ² g ⁻¹)	Intrinsic H ₂ evolution rate‡ (μmol h ⁻¹ m ⁻²)
Urea-CN _x	2.86	56.2	17.9	64.6	43.5
NCN-CN _x	2.69	24.7	9.3	54.9	22.5
Melon	2.69	2.0	0.5	16.4	6.1
Melon (urea)	2.74	4.4	4.7	42.3	5.2

*Determined from Figure S3

**AM1.5 irradiation, 20 mg photocatalyst, optimized platinum loading and MeOH (20 mL of 10 vol%) as electron donor

†As in *, but using 400±20 nm band pass filter

‡Normalizing the final steady rate of hydrogen evolution under AM1.5 (column 3) with BET surface area (column 5) taking into account that 20 mg of photocatalyst was used in each experiment

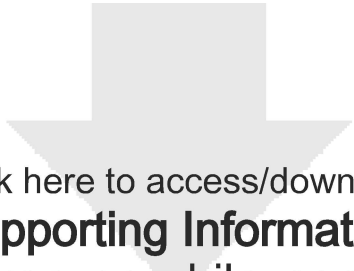
Table S4 Comparison of the photocatalytic activity for hydrogen evolution, based on AQE values, of the carbon nitrides synthesized in this work and selected visible light active photocatalysts from our group and from the literature.

Photocatalyst	Catalyst loading (mg mL ⁻¹)	AQE (%)	λ (nm)	Reactant solution
Pt/Urea-CN _x	1	18	400	MeOH
Pt/NCN-CN _x	1	9	400	MeOH
Pt/Melon (this work)	1	0.5	400	MeOH
Pt/Melem oligomer ^[6]	1	1	400	MeOH
Pt/Poly(triazine imide) ^[10]	1	Inactive	-	MeOH
Pt/Poly(triazine imide) ^[10]	1	0.6	400	Triethanolamine
Pt/Poly(triazine imide), 4-amino-2,6-dihydroxypyrimidine doped ^[10]	1	0.3	400	MeOH
Pt/Poly(triazine imide), 4-amino-2,6-dihydroxypyrimidine doped ^[10]	1	3	400	Triethanolamine
Pt/Azine COF ^[11]	0.5	Inactive	-	MeOH
Pt/Azine COF ^[11]	0.5	0.5	450	Triethanolamine
Pt/Melon (urea) ^[7]	0.43	27	400	Triethanolamine
Pt/Melon hollow nanosphere ^[12]	0.2	7.5	420	Triethanolamine
Pt/Poly(triazine imide), 2,4,6-triaminopyrimidine doped ^[13]	1	15	400	Triethanolamine
Pt/CdS ^[14]	26	35	436	Na ₂ SO ₃
Pt/AgInZn ₇ S ₉ ^[14]	1	20	420	Na ₂ S + K ₂ SO ₃
Rh _{2-x} Cr _x O ₃ / (Ga _{0.88} Zn _{0.12})(N _{0.88} O _{0.12}) ^[14]	0.81	6	420-440	H ₂ SO ₄ (pH 4.5)

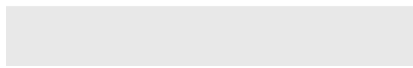
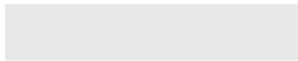
References

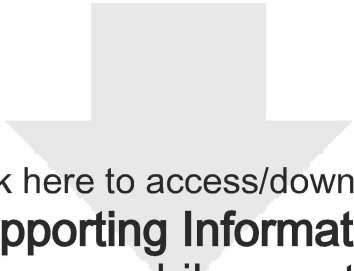
- [1] B. M. Fung, A. K. Khitrin, K. Ermolaev, *J. Magn. Reson.* **2000**, *142*, 97-101.
- [2] a) B.-J. v. Rossum, H. Förster, H. J. M. d. Groot, *J. Magn. Reson.* **1997**, *124*, 516-519;
b) A. Lesage, L. Emsley, *J. Magn. Reson.* **2001**, *148*, 449-454.
- [3] D. Massiot, F. Fayon, M. Capron, I. King, S. L. Calvé, B. Alonso, J.-O. Durand, B. Bujoli, Z. Gan, G. Hoatson, *Magn. Reson. Chem.* **2002**, *40*, 70-76.
- [4] a) R. Sangill, N. Rastrupandersen, H. Bildsoe, H. J. Jakobsen, N. C. Nielsen, *J. Magn. Reson., Ser A* **1994**, *107*, 67-78; b) C. Gervais, F. Babonneau, J. Maquet, C. Bonhomme, D. Massiot, E. Framery, M. Vaultier, *Magn. Reson. Chem.* **1998**, *36*, 407-414; c) C. Gervais, J. Maquet, F. Babonneau, C. Duriez, E. Framery, M. Vaultier, P. Florian, D. Massiot, *Chem. Mater.* **2001**, *13*, 1700-1707.
- [5] a) J. Schaefer, T. A. Skokut, E. O. Stejskal, R. A. McKay, J. E. Varner, *Proc. Natl. Acad. Sci. U.S.A.* **1981**, *78*, 5978-5982; b) J. Schaefer, E. O. Stejskal, J. R. Garbow, R. A. McKay, *J. Magn. Reson.* **1984**, *59*, 150-156; c) M. Baldus, A. T. Petkova, J. Herzfeld, R. G. Griffin, *Mol. Phys.* **1998**, *95*, 1197-1207.
- [6] V. W.-h. Lau, M. B. Mesch, V. Duppel, V. Blum, J. Senker, B. V. Lotsch, *J. Am. Chem. Soc.* **2015**, *137*, 1064-1072.
- [7] D. J. Martin, K. Qiu, S. A. Shevlin, A. D. Handoko, X. Chen, Z. Guo, J. Tang, *Angew. Chem.* **2014**, *53*, 9240-9245.
- [8] V. W.-h. Lau, I. Moudrakovski, T. Botari, S. Weinberger, M. B. Mesch, V. Duppel, J. Senker, V. Blum, B. V. Lotsch, *Nat. Commun.* **2016**, *7*, 12165.
- [9] J. Melke, B. Peter, A. Habereeder, J. Ziegler, C. Fasel, A. Nefedov, H. Sezen, C. Wöll, H. Ehrenberg, C. Roth, *ACS Appl. Mater. Interfaces* **2016**, *8*, 82-90.

- 1
2
3 [10] K. Schwinghammer, B. Tuffy, M. B. Mesch, E. Wirnhier, C. Martineau, F. Taulelle,
4
5 W. Schnick, J. Senker, B. V. Lotsch, *Angew. Chem. Int. Ed.* **2013**, *52*, 2435-2439.
6
7
8 [11] V. S. Vyas, F. Haase, L. Stegbauer, G. Savasci, F. Podjaski, C. Ochsenfeld, B. V.
9
10 Lotsch, *Nat. Commun.* **2015**, *6*, 8508.
11
12 [12] J. Sun, J. Zhang, M. Zhang, M. Antonietti, X. Fu, X. Wang, *Nat. Commun.* **2012**, *3*,
13
14 1139.
15
16 [13] M. K. Bhunia, K. Yamauchi, K. Takanabe, *Angew. Chem. Int. Ed.* **2014**, *53*, 11001-
17
18 11005.
19
20 [14] A. Kudo, Y. Miseki, *Chem. Soc. Rev.* **2009**, *38*, 253-278.
21
22
23
24
25
26
27
28
29
30
31
32
33
34
35
36
37
38
39
40
41
42
43
44
45
46
47
48
49
50
51
52
53
54
55
56
57
58
59
60
61
62
63
64
65

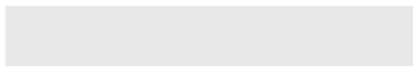
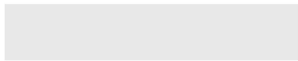


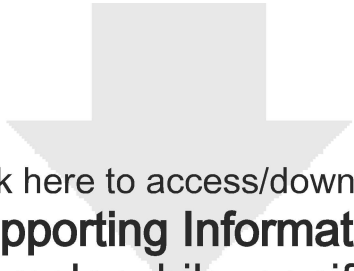
Click here to access/download
Supporting Information
urea_cnx_bilayer.cif



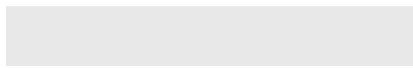
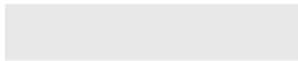


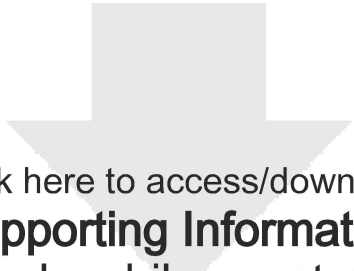
Click here to access/download
Supporting Information
urea_cnx_bilayer_pt.cif



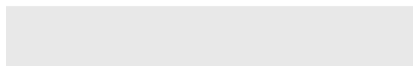
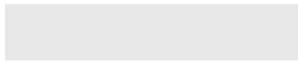


Click here to access/download
Supporting Information
melon_bilayer.cif





Click here to access/download
Supporting Information
melon_bilayer_pt.cif









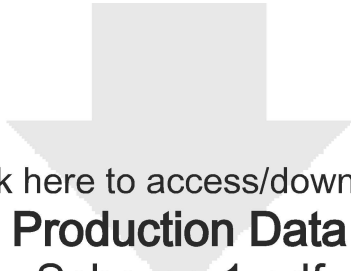









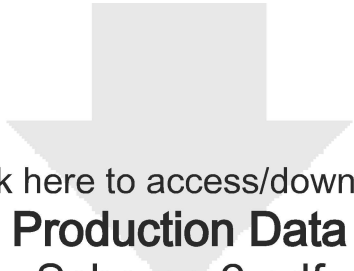




Click here to access/download

Production Data
Scheme 1.pdf





Click here to access/download

Production Data
Scheme 2.pdf

